

Numerical Simulations of Liquid Metal MHD Flows at Very High Hartmann Number

Mohammadali Areekkadan

A Thesis Submitted to
Indian Institute of Technology Hyderabad
In Partial Fulfillment of the Requirements for
The Degree of Master of Technology



Department of Mechanical and Aerospace Engineering

July 2014

Declaration

I declare that this written submission represents my ideas in my own words, and where ideas or words of others have been included, I have adequately cited and referenced the original sources. I also declare that I have adhered to all principles of academic honesty and integrity and have not misrepresented or fabricated or falsified any idea/data/fact/source in my submission. I understand that any violation of the above will be a cause for disciplinary action by the Institute and can also evoke penal action from the sources that have thus not been properly cited, or from whom proper permission has not been taken when needed.



(Signature)

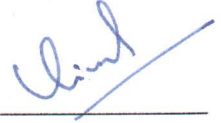
(Mohammadali Areekkadan)

ME12M1015

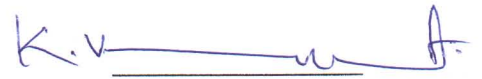
(Roll No.)

Approval Sheet

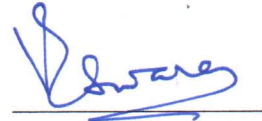
This Thesis entitled Numerical Simulation of Liquid Metal MHD Flows at Very High Hartmann Number by Mohammadali Areekkadan is approved for the degree of Master of Technology from IIT Hyderabad



(Dr. Vinod Janardhanan) Examiner
Dept. of Chemical Engineering
IITH



(Dr. K. Venkatasubbaiah) Examiner
Dept. of Mechanical and Aerospace Eng
IITH



(Prof. Vinayak Eswaran) Adviser
Dept. of Mechanical and Aerospace Eng
IITH

Acknowledgements

I express my sincere gratitude to my supervisor Professor Prof. V. Eswaran for his valuable guidance, timely suggestions and constant encouragement. His interest and confidence in me has helped immensely for the successful completion of this work. I would like to extend my sincere thanks to T. Praveen for his continuous support and suggestive discussions. I am also thankful to Narendra Gajbhiye, Ashwani, Nikhil R for their suggestions, generous help and for maintaining friendly ambiance in the Heat Transfer Lab. I would like to make a special mention of the excellent computational facilities provided by IIT Hyderabad. Finally, I would like to thank my parents and my siblings for their constant support and encouragement.

Mohammadali Areekkadan

To my parents ...

Abstract

Magnetohydrodynamics flows are those which involves the interaction between the flow of electrically conducting fluids and electromagnetic fields. Such flows are governed by Navier-Stokes, continuity along with Maxwell's equations, and are commonly encountered in applications of practical interest.

In the first part of the thesis validations of ANUPRAVAHA MHD module were carried out with available analytical results. In the second part of the thesis numerical simulations of MHD rectangular duct flow were carried out for various arbitrary wall conductance ratio and Hartmann number using induction-less formulation and results of velocity profile and pressure gradient have presented.

In the final part of the thesis fully developed MHD flow solution in a rectangular duct has been investigated to obtain flow profile and pressure gradient at very high Hartmann number (order of 10^4) using inertia-less formulation. The results of the study compared with solution from numerical simulation of full set of equation and shows good agreement. In this method computation time for simulation was reduced considerably because of the lesser grid point and neglecting the non-linear term in the momentum equation.

Contents

Declaration	ii
Approval Sheet	iii
Acknowledgements	iv
Abstract	vi
Nomenclature	viii
1 Introduction	1
1.1 Application	2
1.1.1 MHD flow meter	2
1.1.2 Electromagnetic pump	2
1.1.3 MHD generator	3
1.1.4 Liquid metal flow in fusion blanket	4
1.2 Literature review	4
1.3 About the solver: ‘ANUPRAVAHA’	5
1.4 Statement of objectives	6
1.5 Structure of report	6
2 Theoretical Background	7
2.1 Assumptions	7
2.2 Electromagnetism	8
2.2.1 Maxwell’s equations	8
2.2.2 Charge continuity equation	8
2.2.3 Ohm’s Law	9
2.2.4 The Magnetic Induction Equation	9
2.3 Fluid Mechanics	10
2.3.1 Continuity Equation	10
2.3.2 Momentum Equation	10
2.4 Dimensionless Groups	11

2.5	The quasi-static approximation	12
2.6	Poisson equation for electrical potential	14
2.7	Initial and Boundary Conditions	14
2.7.1	Initial Condition	14
2.7.2	Boundary Condition	14
2.8	The Solver-a brief algorithm	16
2.9	Fundamental Phenomena in MHD duct flow	17
3	Code Validation	20
3.1	Flow between parallel planes - Hartmann flow	20
3.1.1	Hartmann flow with insulating walls	21
3.1.2	Hartmann flow with perfectly conducting walls	22
3.2	Buoyancy driven convection in a rectangular cavity	23
3.3	MHD flow in rectangular duct-Hunt's solution	27
4	MHD flow through rectangular duct- effect of wall conductivity	30
4.1	Laminar MHD flow in straight rectangular duct	30
5	MHD flow in rectangular duct-fully developed solution	36
5.1	Formulation of the problem	36
5.2	Boundary conditions and input parameters	38
5.3	Grid and Computational detail	39
5.4	Comparison with full solution	39
5.5	Fully developed flow solution at very high Hartmann number	43
6	Conclusion	50
	References	52

Chapter 1

Introduction

Magnetohydrodynamics is the branch of physics which studies the interaction between the flow of electrically conducting fluids and electromagnetic fields. It is an interdisciplinary science which is a combination of two familiar sciences: fluid dynamics which is a study of the flow of gases and liquids, and electromagnetism which provides relationships between electric and magnetic fields and current. In MHD fluid must be electrical conducting and non-magnetic, this covers the wide range of materials from electrolytes and liquid metals to partially or fully ionized gases.

The dynamics in an MHD flow can be summarized as follows. The mutual interaction of magnetic field (\mathbf{B}) and velocity field (\mathbf{u}) arises partially as a result of the laws of Faraday and Ampere, and partially because of the Lorentz force experienced by a current-carrying body. It is convenient to split the process into three parts.

- (i) The relative movement of a conducting fluid and a magnetic field causes an e.m.f. (of order $|\mathbf{u} \times \mathbf{B}|$) to develop in accordance with Faraday's law of induction. In general, electrical currents will arise, the current density being of order $\sigma(\mathbf{u} \times \mathbf{B})$, σ being the electrical conductivity.
- (ii) This induced current according to Ampere's law, give rise a induced magnetic field. This adds to the original magnetic field and the change is usually such that the fluid appears to drag the magnetic field lines along with it .
- (iii) The combined magnetic field (imposed plus induced) interacts with the induced current density(\mathbf{J}), to give rise to a Lorentz force $\mathbf{J} \times \mathbf{B}$ (per unit volume). This acts on the conductor and is generally directed so as to prevents the relative movement of the magnetic field and the fluid.

Magnetohydrodynamics applies to a large variety of phenomena like in the spontaneous generation of the Earth's magnetic field by the motion of the liquid iron core of the Earth, in engineering problems such as plasma confinement, liquid-metal cooling of nuclear reactors and electromagnetic casting.

1.1 Application

MHD effects are in several industrial process as well as in technical devices. Some application related to duct and channel flows are given below.

1.1.1 MHD flow meter

The working principle of an MHD flow meter is shown in Fig. 1.1. In an electrically conducting fluid flowing in a pipe and subject to an external magnetic field perpendicular to the flow direction an electrical voltage is induced, which can be sensed by a voltmeter. The measured voltage is proportional to the volumetric flow rate. This measuring principle is suitable even for liquids with low electrical conductivities such as ordinary tap water.

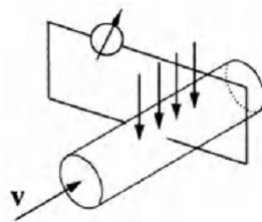


Figure 1.1: Working principle MHD flow meter

1.1.2 Electromagnetic pump

Electromagnetic pump or conduction pump is a type of pump in which the liquid is moved by electromagnetic force. Working principle is shown in Fig. 1.2. The electrical current \mathbf{I} through the liquid in the duct interacts with the externally applied magnetic field \mathbf{B} and generates an induced electromagnetic force (Lorentz force) which drive the liquid through the pipe. Usually large electric current is require to get adequate volumetric flow rate. Conduction pumps are used in industry for delivery of various electrically conducting liquids, particularly for conveying and pouring molten metals.

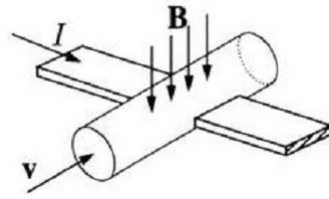


Figure 1.2: Working principle Conduction Pump

1.1.3 MHD generator

Magnetohydrodynamics power generation provides a way of generating electricity directly from a fast moving stream of ionized gases without the need for any moving mechanical parts. The working principle is shown in Fig. 1.3. The MHD generator can be considered as fluid dynamo. This is similar to a mechanical dynamo in which the motion of a metal conductor through a magnetic field creates a current in the conductor except that in the MHD generator the metal conductor is replaced by a conducting gas plasma. A highly pressurized and extremely hot (3500K) and thus ionized gas is expanded through a nozzle which is subject to a strong external magnetic field. In the ionized gas flow a charge separation occurs under the effect of the imposed magnetic field and an electrical potential difference is induced between electrodes inserted in channel wall sections aligned with the direction of the magnetic field. This MHD power process utilized as a topping cycle in a combined thermal power plant gives a potential for high overall thermal efficiencies.

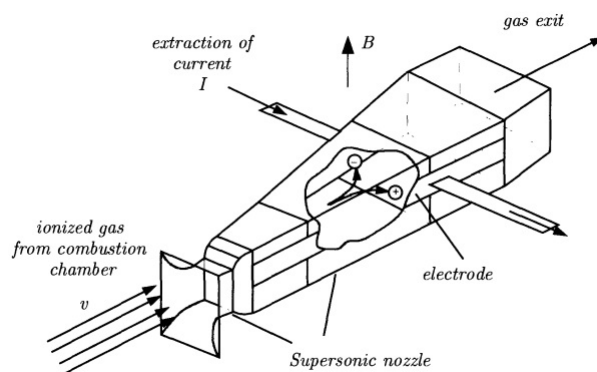


Figure 1.3: Working principle MHD Generator

1.1.4 Liquid metal flow in fusion blanket

Magnetohydrodynamic (MHD) flows play an important role in liquid-metal cooled fusion reactor blankets. The reaction between a deuterium and tritium core can only take place if both reactants are completely ionized. These ionized plasmas are characterized by very high conductivities and densities. Intense magnetic fields are used to confine these plasmas within the reaction vessel. To protect associated devices of fusion reactor from this high energy plasma some blanket module are used. These blankets are multi functional: in the first place, they should absorb the neutron flux and convert the kinetic energy of the neutrons into heat, which can then be used to drive a classical turbine process. Liquid metals are candidate coolant liquids since they can be operated at high temperature and have high thermal conductivities. The second function of the blankets is to protect the magnetic field coils from intense, damaging neutron radiation. In more advanced blanket designs (called self-cooling blankets), the liquid coolants also have to provide the tritium needed for the fusion reaction. This is possible if the coolant contains lithium. Liquids that are considered are pure lithium or eutectic lead-lithium alloy. Due to MHD effect these blanket are subjected to huge pressure drop, turbulence modifications, changes in heat and mass transfer and other important MHD phenomena.

1.2 Literature review

Liquid metal MHD received the attention of researchers starting with the pioneering work of Hartmann (1937) in liquid metal duct flow in the presence of a strong external magnetic field. Shercliff(1952,1956) [13] studied steady, viscous motion of electrically conducting fluid in the presence of imposed transverse magnetic field in circular pipe with insulating and conducting wall. Chang *et.al* [1] gave an analytical solution for the velocity and induced magnetic field for the case of Hartmann flow. Hunt [2] presented an analysis of laminar motion of a conducting liquid in a rectangular duct under a uniform transverse magnetic field. He presented exact solutions for two cases(i) perfectly conducting walls perpendicular to the field and thin walls of arbitrary conductivity parallel to the field, and (ii) non-conducting walls parallel to the field and thin walls of arbitrary conductivity perpendicular to the field. He obtained an M-shaped velocity profile having a large velocity near the insulating walls. He also carried out theoretical analysis on three dimensional MHD duct flows with obstacles in the flow field under the influence of a very strong magnetic field in which

he showed that the flow over an obstacle is highly dependent on the conductivity of the duct walls as well as on the conductivity of the body .

MHD flows at high hartmann number have been studied extensively by the method of asymptotic expansion. Walker [3] gave review of these result. Asymptotic analysis is based on the assumption on the order of magnitude in the different terms in the governing equation. Generally inertia and viscous friction are neglected. These kinds of assumptions can lead to results which are not valid for the parameters which are characteristic of the fusion blanket. Therefore, semi-analytical or semi-numerical methods have been developed Talmage *et.al.* (1988).

The influence of a magnetic field on the heat transfer in buoyancy driven flows in case of crystal growth and breeding blankets of fusion reactors has been studied by several authors. Garandet *et.al.* [4] proposed an analytical solution to the equations of magnetohydrodynamics for a case of buoyancy driven convection in a two dimensional cavity under the influence of a transverse magnetic field. Ben Hadid *et.al.* [5] carried out a study on the convection in a horizontal bridgman configuration under the influence of a constant magnetic field in case of two and three-dimensional flow. Ozoe *et.al.* [6] numerically studied the effect of the direction of the external magnetic field on the three-dimensional natural convection in a cubical enclosure. Piazza *et.al.*[7] have numerically simulated free convection in a differentially heated and volumetrically heated cubic enclosure. Karcher *et.al.* [8] conducted experimental and numerical studies on natural convection in a cylindrical test cell filled with liquid alloy Gallium-Indium-Tin (GaInSn), heated locally at its upper surface and affected by a vertical magnetic field. The text book on liquid metal MHD flows in containers by Muller *et. al.*[9] discusses broadly on internal flows of liquid metals which are of industrial importance.

1.3 About the solver: ‘ANUPRAVAHA’

ANUPRAVAHA, a robust general purpose CFD solver created during an earlier BRNS funded IITK-DAE project (2004-2009)for use at BARC and associated institutions. The code (ANUPRAVAHA), written in C, is a multi-block finite-volume solver for non-orthogonal hexahedral structured grids has been in continuous development ever since. Apart from the basic module for the Navier-Stokes, Temperature and species transport equations, the solver is now capable of solving problems with Conjugate Heat Transfer, thermal Radiation with participating media, Multiphase and Droplet-dispersed phase flows, Variable density flows, Combustion, Liquid metal MHD, Tur-

bulence, and solidification-melting, in arbitrarily complex geometries. The code reads mesh file and write solution in CGNS format which can be post-processed in most of commercial as well as open-source post-processing packages.

1.4 Statement of objectives

The objectives of this thesis are

- Validate Anupravaha MHD module with available analytical solutions.
- Numerical simulation of MHD flow in rectangular ducts to study the effect of wall conductivity on pressure drop and flow field using electrical potential formulation of Anupravaha solver.
- Numerical simulation of MHD flow in rectangular duct in fully developed region using the inertia-less formulation of Anupravaha solver at very high Hartmann number ($\sim 10^4$) and calculation of pressure gradient for arbitrary wall conductivity.

1.5 Structure of report

This report is organized in the following way. Chapter 2 deals with theoretical background of MHD which include governing equations, assumptions, dimension-less numbers and a brief introduction to Anupravaha MHD solver algorithm. In Chapter 3 validation of solver for various test cases are outlined. Chapter 4 discuss effect of wall conductivity on MHD pressure drop in a rectangular duct for different Hartmann number by solving full equations using electrical potential formulation of the solver. Chapter 5 deals with numerical simulation of MHD flow in rectangular duct in fully developed region using the inertia-less formulation of Anupravaha solver at very high Hartmann number and calculation of pressure gradient for arbitrary wall conductivity.

Chapter 2

Theoretical Background

Liquid metal flows under the influence of a magnetic field are governed by the Navier-Stokes equations and electrodynamic equations. The equations which are to be solved for numerically simulating these flows are derived from different electrodynamic equations like Maxwell's equations, Amperes law, Ohm's law and charge conservation. If the induced magnetic field is not strong enough to perturb the imposed magnetic field it is enough to solve Navier-Stokes equation along with a Poisson equation for the electric potential, However, if the induced magnetic field is strong then along with these equations one should solve a vector equation (with solenoidal constraint) for the induced magnetic field.

In this chapter various governing equations, assumptions, non dimensional numbers related to MHD, boundary conditions, and fundamental phenomena in MHD duct flow are described. The discussion of this chapter owes substantially to N.Vetcha[11]

2.1 Assumptions

- Flow is laminar, incompressible, and Newtonian.
- The fluid is electrically conducting and non-magnetic.
- Unless otherwise mentioned, it is assumed that the material properties are constant.

2.2 Electromagnetism

2.2.1 Maxwell's equations

The pillars of classical electromagnetism are described by Maxwells equations, which simplified for magnetohydrodynamics conditions are:

1. Gauss's law of electric field

$$\nabla \cdot \mathbf{E} = \frac{\rho_e}{\epsilon_0} \quad (2.1)$$

2. Gauss's law of magnetism

$$\nabla \cdot \mathbf{B} = 0 \quad (2.2)$$

3. Faraday's law of induction

$$\nabla \times \mathbf{E} = -\frac{\partial \mathbf{B}}{\partial t} \quad (2.3)$$

4. Ampere's-Maxwell equation

$$\nabla \times \mathbf{B} = \mu_m(\mathbf{J} + \epsilon_0 \frac{\partial \mathbf{E}}{\partial t}) \quad (2.4)$$

where \mathbf{E} is the electric field, \mathbf{B} the magnetic field strength, \mathbf{J} the current density, ϵ_0 the electric permittivity ρ_e the charge density and μ_m is the magnetic permeability of the medium.

2.2.2 Charge continuity equation

As given in previous section Ampers-Maxwell equation(2.4) is

$$\nabla \times \mathbf{B} = \mu_m(\mathbf{J} + \epsilon_0 \frac{\partial \mathbf{E}}{\partial t}) \quad (2.5)$$

The above equation is capable of describing a great range of phenomena like electromagnetic waves. The last term in (2.5) was introduced by Maxwell as a correction to Ampere's law and is called the displacement current; it is introduced to account for the conservation of charge. However, this correction is not needed in MHD, because under MHD approximation speeds are very small compared with the speed of light c .

$$\frac{\mu_m \epsilon_0 \frac{\partial \mathbf{E}}{\partial t}}{\nabla \times \mathbf{B}} \approx \left(\frac{u}{c}\right)^2 \ll 1$$

Therefore we can use the pre-Maxwell form of (2.5), which is simply the Ampere's law in differential form.

$$\nabla \times \mathbf{B} = \mu_m \mathbf{J} \quad (2.6)$$

Applying divergence to the above equation leads to

$$\nabla \cdot \mathbf{J} = 0 \quad (2.7)$$

The above equation (2.7) is called charge-continuity equation.

2.2.3 Ohm's Law

Ohm's Law states that the total electric current flowing in a conductor is proportional to the total electric field. In addition to the field \mathbf{E} acting on a fluid at rest, a fluid moving with velocity \mathbf{u} in the presence of a magnetic field \mathbf{B} is subject to an additional electric field $\mathbf{u} \times \mathbf{B}$. Ohm's law then gives

$$\mathbf{J} = \sigma(\mathbf{E} + \mathbf{u} \times \mathbf{B}) \quad (2.8)$$

2.2.4 The Magnetic Induction Equation

If we combine Ohm's law(2.8), Faraday's equation(2.3) and Ampere's law (2.4) we obtain an expression relating \mathbf{B} to \mathbf{u}

$$\frac{\partial \mathbf{B}}{\partial t} = -\nabla \times \mathbf{E} = -\nabla \times [(\mathbf{J}/\sigma) - \mathbf{u} \times \mathbf{B}] = \nabla \times [\mathbf{u} \times \mathbf{B} - \nabla \times \mathbf{B}/\mu_m \sigma]$$

noting that $\nabla \times \nabla \times \mathbf{B} = -\nabla^2 \mathbf{B}$ (since \mathbf{B} is solenoidal), this simplifies to

$$\frac{\partial \mathbf{B}}{\partial t} = \nabla \times (\mathbf{u} \times \mathbf{B}) + \lambda \nabla^2 \mathbf{B} \quad (2.9)$$

where $\lambda \equiv 1/\mu_m \sigma$ is called the magnetic diffusivity . The equation(2.9) is also known as the transport or advection-diffusion equation for \mathbf{B} , where \mathbf{B} now is the total magnetic field which includes both the imposed and the induced magnetic fields. However as the former is usually constant, the equation effectively computes the induced magnetic field. As the Eqn(2.9) is linear, the imposed component of \mathbf{B} may be subtracted out of the equation which then could be used to compute only the induced field (with BC for the induced field). Equation (2.9) describes the evolution of the magnetic field \mathbf{B} . The first term on the right-hand side is the induction term

that describes the interaction of the field with the flow \mathbf{u} . It is the only term that can generate field. The second term on the right-hand side is a diffusive term. Using the fact that \mathbf{B} is solenoidal and that the fluid is incompressible, $\nabla \cdot \mathbf{u} = 0$ we can get the following modified form of the induction equation.

$$\frac{\partial \mathbf{B}}{\partial t} + (\mathbf{u} \cdot \nabla) \mathbf{B} = \lambda \nabla^2 \mathbf{B} + (\mathbf{B} \cdot \nabla) \mathbf{u} \quad (2.10)$$

2.3 Fluid Mechanics

2.3.1 Continuity Equation

The general continuity equation is

$$\frac{\partial \rho}{\partial t} + \nabla \cdot (\rho \mathbf{u}) = 0 \quad (2.11)$$

For incompressible flow continuity equation reads as

$$\nabla \cdot \mathbf{u} = 0 \quad (2.12)$$

2.3.2 Momentum Equation

The Navier Stokes equations for laminar incompressible MHD flow of a Newtonian fluid, can be written as

$$\rho \left[\frac{\partial \mathbf{u}}{\partial t} + (\mathbf{u} \cdot \nabla) \mathbf{u} \right] = -\nabla p + \nu \rho \nabla^2 \mathbf{u} + \mathbf{f} + \mathbf{J} \times \mathbf{B} \quad (2.13)$$

where p denotes the pressure, ρ the fluid mass density, ν its kinematic viscosity. The interpretation is obvious. The temporal evolution of the linear momentum of a fluid element changes by the action of pressure force, $-\nabla p$, viscous friction, $\rho \nu \nabla^2 \mathbf{u}$, by volumetric forces \mathbf{f} of non-electromagnetic origin like gravity and by the occurrence of Lorentz (or Laplace forces), $\mathbf{j} \times \mathbf{B}$. Lorentz forces couple the mechanical and electrodynamic states of the system. Lorentz forces act in planes perpendicular to current and magnetic field vectors.

Using Ampere's law (2.4) the Lorentz forces can be written in the form of the divergence of a stress tensor, the so-called Maxwell stress tensor. It plays an important role in some technical arrangements such as in liquid metal processing. Introducing Ampere's law in the expression for the Lorentz force we get after some analytical

manipulation

$$\mathbf{j} \times \mathbf{B} = -\frac{1}{\mu} \mathbf{B} \times \nabla \times \mathbf{B} = -\nabla \left(\frac{1}{2\mu} \mathbf{B}^2 \right) + \frac{1}{\mu} \nabla \cdot (\mathbf{B}\mathbf{B}) \quad (2.14)$$

where $(\mathbf{B}\mathbf{B})$ is the dyadic product of vector \mathbf{B} with itself. The first term of right hand side of equation(2.14) is gradient of scalar so we can call this part as *magnetic pressure*.while the last term describes a stress term called *Maxwell's stress*.

2.4 Dimensionless Groups

It is useful to present the governing equation(2.13,2.17,2.12) in dimensionless form by using the following substitutions $u^* = u/U, B^* = B/B_0, \nabla^* = L^{-1}\nabla, t^* = tU/L, J^* = J/\sigma UB_0, p^* = p/\rho U^2$ and omitting star after substitution, we obtain

$$\nabla \cdot \mathbf{u} = 0 \quad (2.15)$$

$$\frac{\partial \mathbf{u}}{\partial t} + (\mathbf{u} \cdot \nabla) \mathbf{u} = -\nabla p + Re^{-1} \nabla^2 \mathbf{u} + \mathbf{f} + \mathbf{N}(\mathbf{J} \times \mathbf{B}) \quad (2.16)$$

$$\frac{\partial \mathbf{B}}{\partial t} + (\mathbf{u} \cdot \nabla) \mathbf{B} = R_m^{-1} \nabla^2 \mathbf{B} + (\mathbf{B} \cdot \nabla) \mathbf{u} \quad (2.17)$$

$$\nabla \cdot \mathbf{B} = 0 \quad (2.18)$$

We see that, in a given geometry, we can characterize MHD flows by mainly three dimensionless groups: the *Reynolds number* \mathbf{Re} , the *interaction parameter*(or Stuart number) \mathbf{N} , and the *magnetic Reynolds number* \mathbf{Rm} . The definition and physical meaning of these parameters is discussed below.

The Reynolds number is a non-dimensional estimate of the ratio between convective and viscous forces in the Navier-Stokes equation ($\mathbf{Re} = \frac{\mathbf{UL}}{\nu}$). If the Reynolds number is small, small-scale fluctuations can not overcome the dissipative action of the viscous forces, and will quickly be damped. This results in a homogenized flow in which only slow variations of the velocity field are possible. At large Reynolds number however, small-scale fluctuations can persist and grow due to the increasing impact of the (non-linear) convective term. This will give rise to a seemingly random behavior that is characterized by a large range of spatial temporal scales, a state known as *turbulence*.

The analogous ratio between convective and diffusive terms in the magnetic induction equation is known under the name *magnetic Reynolds number*, and is defined

as

$$R_m = \mu\sigma UL$$

The phenomenology of MHD systems will depend strongly on the value of R_m , as it is the only parameter governing the induction equation. When R_m is small, magnetic field fluctuations relax quickly; velocity inhomogeneities, which are at the origin of these fluctuations, hardly affect the magnetic field. Such flows have a dissipative nature; the kinetic energy of the fluid is transformed into heat due to Joulean dissipation. Small values of the magnetic Reynolds number are typical for man made flows, like the ones encountered in laboratory and industrial processes. High values of R_m , on the other hand are typical for large-scale terrestrial or astrophysical flows. Such flows are such that the magnetic field is 'frozen' into the fluid, and can exhibit wave-like behavior.

The interaction parameter is a measure for the ratio between electromagnetic and inertial forces. It reads as.

$$N = \frac{\sigma B_0^2 L}{\rho U}$$

It is also important to interpret this parameter as the ratio between two time scales. On the one hand, there is the Joule damping time, τ_J which is the typical time needed by the Lorentz force to damp a vortex. It is given by: $\tau_J = \rho/\sigma B_0^2$. On the other hand, we have the eddy-turnover time τ_e which is the time scale on which a vortex moves over a typical length scale L : $\tau_e = L/U$, and we can write the interaction parameter as

$$N = \frac{\tau_e}{\tau_J}$$

Hartmann number (**Ha**), a fourth parameter which is hybrid of Re and N , is the ratio of square root of electro magnetic force to viscous force and can be read as,

$$\mathbf{Ha} = B_0 L \sqrt{\frac{\sigma}{\mu}} = \sqrt{\mathbf{N} \mathbf{Re}}$$

2.5 The quasi-static approximation

In the previous section, we found that the induction equation (2.17) contains only one non-dimensional group: the magnetic Reynolds number R_m , for most terrestrial, laboratory and industrial flows, this parameter is typically small compared to one. The assumption that R_m is vanishing, allows for a substantial simplification of the MHD equations. Consider therefore equation (2.17), in which we decompose the

magnetic field in a uniform, stationary, externally imposed part \mathbf{B}^{ext} and a fluctuating part \mathbf{b} . So equation (2.17) becomes

$$\frac{\partial \mathbf{b}}{\partial t} + u \cdot \nabla \mathbf{b} = \mathbf{B}^{ext} \cdot \nabla u + \mathbf{b} \cdot \nabla u + \frac{1}{\mu\sigma} \nabla^2 \mathbf{b} \quad (2.19)$$

An order-of-magnitude estimate of the convective and diffusive terms gives

$$\frac{\mathcal{O}(u \cdot \nabla \mathbf{b})}{\mathcal{O}((\mu\sigma)^{-1} \nabla^2 \mathbf{b})} = \frac{U b L^{-1}}{(\mu\sigma)^{-1} b L^{-2}} = R_m \quad (2.20)$$

where b is a typical scale of the fluctuating magnetic field. We can thus neglect the second term on both the right and left-hand side of equation (2.19). This leads to

$$\frac{\partial \mathbf{b}}{\partial t} = \mathbf{B}^{ext} \cdot \nabla u + \frac{1}{\mu\sigma} \nabla^2 \mathbf{b} \quad (2.21)$$

This is a diffusion equation with a source term due to gradients in the velocity field. We can now pursue our analysis by considering the time scales associated with both terms on the right-hand side. The ratio between these is

$$\frac{\tau((\mu\sigma)^{-1} \nabla^2 \mathbf{b})}{\mathbf{B}^{ext} \cdot \nabla u} = \frac{L^2 \mu\sigma}{L U^{-1}} = R_m \quad (2.22)$$

This means that the fast response of the diffusion term makes the magnetic field fluctuations adapt quasi-instantaneously to (slower) variations due to the flow. As such, we end up with the following static equation for the induced magnetic field.

$$\mathbf{B}^{ext} \cdot \nabla u + \frac{1}{\mu\sigma} \nabla^2 \mathbf{b} = 0 \quad (2.23)$$

An order-of-magnitude estimate of this equation leads to the following result

$$\frac{\mathcal{O}(\mathbf{b})}{\mathcal{O}(\mathbf{B}^{ext})} = \mu\sigma U L = R_m \quad (2.24)$$

We find thus that, in the limit of vanishing R_m , the induced magnetic field is negligible with respect to the externally imposed one. So we can neglect the induced magnetic field and its effect and this approach is called *quasi-static* or *induction-less approach*.

2.6 Poisson equation for electrical potential

One another important equation which governs the flow of liquid metal subjected to a magnetic field is Ohm's law (2.8). If the induced magnetic field is small compared to the applied magnetic field, the magnetic field variables need not be solved and with the electric field being curl free, an electric potential such that $E = -\nabla\phi$, where ϕ is the electric potential, the equation (2.8) becomes.

$$\mathbf{J} = \sigma(-\nabla\phi + \mathbf{u} \times \mathbf{B}) \quad (2.25)$$

Using solenoidal nature of electric current and taking divergence of above equation results

$$\nabla^2\phi = \nabla \cdot (\mathbf{u} \times \mathbf{B}) \quad (2.26)$$

2.7 Initial and Boundary Conditions

2.7.1 Initial Condition

Arbitrary initial conditions can be given for those flows in which the induced magnetic field is assumed negligible, these flows commonly end up in a steady state solution. On the other hand if the induced magnetic field is perturbing the imposed magnetic field then proper initial condition on the induced magnetic field is required to get an unsteady, perhaps periodic solution.

2.7.2 Boundary Condition

Boundary condition on flow field

At the wall, no-slip conditions are applicable for all components of velocity. i.e. $u = 0$ and $v = 0$. For temperature, generally Dirichlet (temperature specified) or Neumann (flux-specified) boundary conditions apply at walls, while Dirichlet BC apply at flow inlet and Neumann BC at outlets. Generally uniform inlet boundary condition is used at the inlet. At the exit plane, homogeneous Neumann boundary condition is used for all components of velocity and temperature. A homogeneous Neumann condition is specified for pressure on velocity specified boundaries and a homogeneous Dirichlet pressure condition at the exit plane.

Boundary condition on ϕ

The conductivity of the duct walls decide the boundary conditions on the electric potential ϕ . If the walls are insulating then a homogeneous Neumann condition is used and if the walls are perfectly conducting then a homogeneous Dirichlet boundary condition is used. For arbitrary wall conductivity we will be solving conjugate (solid-fluid) modeling. So the general interface condition for the electric potential applicable for all Quasi-static flows can be derived simply from the fact that the normal component of the current density across the interface must be continuous. This gives

$$\sigma_{fluid} \left(\frac{\partial \phi}{\partial \mathbf{k}} \right)_{fluid} = \sigma_{solid} \left(\frac{\partial \phi}{\partial \mathbf{k}} \right)_{solid}$$

The boundary conditions at entry and the outlet are chosen such that no electric currents leave or enter the domain, this leads to the following

$$\left. \frac{\partial \phi}{\partial \mathbf{n}} \right|_{entry} = 0$$

$$\left. \frac{\partial \phi}{\partial \mathbf{n}} \right|_{outlet} = (\mathbf{u} \times \mathbf{B}) \cdot \hat{\mathbf{n}}$$

This results in a zero normal component of current at the entry and at the outlet.

Boundary condition on \mathbf{B}

The boundary condition of total magnetic field \mathbf{B} is decided by conductivity of wall. If the wall is perfectly conducting we use homogeneous Neumann boundary condition; if it is insulating we use homogeneous Dirichlet boundary condition on the all component of \mathbf{B} on which there is no magnetic field being applied. For walls on which a magnetic field is applied, Dirichlet condition is used for that particular component of \mathbf{B} which is in the direction of magnetic field. At the inlet a homogeneous Dirichlet condition is specified and at outlet homogeneous Neumann boundary condition is given. The former reflects the situation that no induced current exists at the flow inlet and latter represents that the induced current does not change in the flow direction at the flow outlet.

Conjugate (Solid-Fluid) modeling is used for duct walls of arbitrary conductivities, for solving the magnetic field. This requires the specification of an interface condition. A solid-fluid interface condition can be derived for the induction equation

(2.17) realizing its similarity to the temperature equation as follows

$$\frac{\partial \mathbf{B}}{\partial t} + (\mathbf{u} \cdot \nabla) \mathbf{B} = \nabla \cdot \nabla \left(\frac{1}{\lambda} \mathbf{B} \right) + (\mathbf{B} \cdot \nabla) \mathbf{u}$$

under steady state, stationary (no-slip wall) condition the above equation become

$$\nabla \cdot \nabla \left(\frac{1}{\lambda} \mathbf{B} \right) = 0$$

Applying the Gauss-Ostrogradskii theorem at the interface and shrinking the volume to zero, we obtain

$$\frac{1}{\lambda_{fluid}} \left(\frac{\partial \mathbf{B}}{\partial k} \right)_{fluid} = \frac{1}{\lambda_{solid}} \left(\frac{\partial \mathbf{B}}{\partial k} \right)_{solid}$$

2.8 The Solver-a brief algorithm

The MHD module of ANUPRAVAHA is capable of solving the coupled mechanical-electromagnetic system and it allows a choice for selecting either the Potential or the Induction method, for the quasi-static and magneto static cases, respectively. It also has an option for including the temperature equation in the computations, for both the flow and solid regions (conjugate heat transfer). A brief algorithm of MHD module is given below.

Initial condition for the velocity and pressure are prescribed for all points in the domain. Initial volume fluxes are calculated. For the induction method, the total magnetic field vector is initialized and the initial magnetic flux is calculated while for the potential method, current fluxes are initialized and the applied magnetic field is specified. Appropriate boundary conditions are given to start the solution.

1. Initially assign the volume flux, $F_f^* = F_f^n$. The Lorentz force source term, $\mathbf{j} \times \mathbf{B}$ is evaluated.
2. The mass-velocities are obtained by integrating the Navier Stokes equation without the pressure gradient term over all the cells till convergence.
3. Calculate volume fluxes, F_{of}^* from mass velocities using linearly interpolated values from cell adjacent centers at each face of the control volume.
4. Iterate the pressure equation with BC till convergence to get pressure p^*
5. Save the old volume fluxes, $(F_f^*)_{prev} = F_f^n$, and evaluate new fluxes as $F_f^* = F_{of}^* - \frac{\Delta t}{\rho} \nabla P_f^* \cdot S_f$

6. Repeat steps 1-5 till convergence of the volume fluxes.
7. Iterate the full N-S equation using the converged flux values to obtain values at the new time step $n+1$ and correct pressure gradient calculated in step 4.

For electrical potential method

- i Calculate $u \times B$ at cell faces through linear interpolation of the newly obtained velocities in step 7 at cell centers.
- ii Evaluate the RHS of the Poisson equation for the electric potential as the sum of face fluxes, $(u \times B)_f \cdot ds_f$
- iii Solve the Poisson equation for the potential with appropriate boundary conditions till convergence.
- iv Calculate the current density and evaluate Lorentz force at cell centers to be used as the source term for the N-S equations as in step 1.

For inertia-less method

In inertia-less method, we need not calculate convection fluxes, so algorithm will be same except in step.2, the mass velocity will be without convection fluxes.

2.9 Fundamental Phenomena in MHD duct flow

Let us consider a fully developed flow in a duct with rectangular cross-section as shown in Fig. 2.1. An electrically conducting fluid is driven through the duct by a constant pressure gradient and flows with unidirectional velocity $\mathbf{v} = u\hat{x}$. The duct and the fluid are exposed to an externally applied magnetic field \mathbf{B} . Walls on which the magnetic field has a normal component are called the *Hartmann walls*, whereas the walls tangential to the field are called the *side walls*. The interaction of the moving fluid with the magnetic field induces an electric field $\mathbf{v} \times \mathbf{B}$ driving the electric current \mathbf{J} . This causes a potential difference between the side walls, as indicated by the symbols \oplus and \ominus in Fig. 2.1. A variation of the potential along the periphery of the duct drives currents along the walls, both inside the walls if they are conducting and inside the viscous layers near the walls, where the induced electric field is weak because of a reduced velocity.

The components of current which are perpendicular to the magnetic field lines induce a Lorentz-force $\mathbf{f}_L = \mathbf{J} \times \mathbf{B}$ In the center of the duct, often called the *core*,

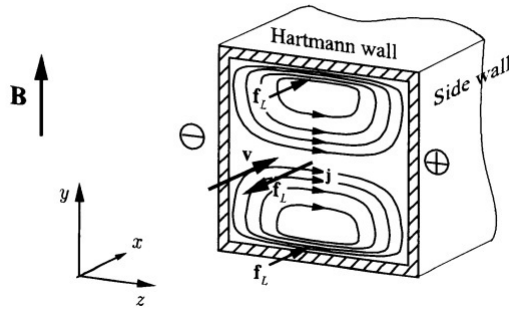


Figure 2.1: Sketch of the MHD channel flow

the Lorentz force acts in the direction opposite to the flow direction and tends to retard the flow. The magnitude of current and as a consequence the magnitude of the Lorentz force depends linearly on the velocity u . If there were regions of higher velocity in the core these would exert stronger braking by the Lorentz force than regions with lower velocities. As a result, the Lorentz force equalizes the fluid flow in the core, where the main balance of forces is established between the Lorentz force and the driving pressure gradient. The Lorentz force contributes therefore to the pressure drop, in addition to the viscous pressure drop in hydrodynamic flow. For strong magnetic fields the electromagnetic pressure drop may exceed the viscous pressure drop by orders of magnitude.

Near the Hartmann walls the velocity drops sharply within thin boundary layers to satisfy the kinematic no-slip boundary condition. These layers are called the Hartmann layers. In regions of low velocity the direction of current is opposite to that in the core. Here the Lorentz force drives the flow against the action of the viscous braking. For strong external magnetic fields the flow in the core turns into a quasi-slug flow with thin boundary layers near the Hartmann walls.

The electric conductivity of the channel walls influences the distribution of current in the fluid and determines the flow pattern. For insulating walls the currents close through the relatively thin Hartmann layers. Because these layers are very thin, their electric resistance is high so that the current magnitude is small. For highly conducting walls a significant fraction of currents may close through the walls in addition to that in the viscous layers. This increases the total magnitude of currents compared to insulating conditions. As a consequence we expect stronger Lorentz forces and a higher pressure drop with increasing wall conductance.

The main purpose of this thesis is to parametrize the pressure drop in rectangular channel against wall conductivity. The flow is assumed to be fully developed, so the

inertia-less approach can be used.

MHD flows very quickly reach fully developed states for uniform flow condition, so it is not necessary to calculate the entrance length to get the pressure drop for practical flow simulation. The assumption of fully developed flow enormously reduces the amount of computation as the flow does not change in the longitudinal direction. This allows us to have only one cell in that direction whereas in developing flows we may need several hundred cells . This allows us to do the computation for for very high Hartmann number flows ($\sim 10^4$), which would otherwise be impossible.

Chapter 3

Code Validation

The majority of theoretical solutions are limited to simple geometries, or otherwise incorporate assumptions like negligible inertial effects. This chapter outlines various validation problem of **ANUPRAVAHA** latest numerical code. All validations are using induction-less (Electrical potential Method) approach.

3.1 Flow between parallel planes - Hartmann flow

Hartmann (1937) first investigated experimentally and theoretically the MHD flow in the gap between two parallel plates. This investigation provided fundamental knowledge for the development of several MHD devices such as MHD pumps, generators, brakes and flow meters. This is a type of MHD flow that corresponds to a general-

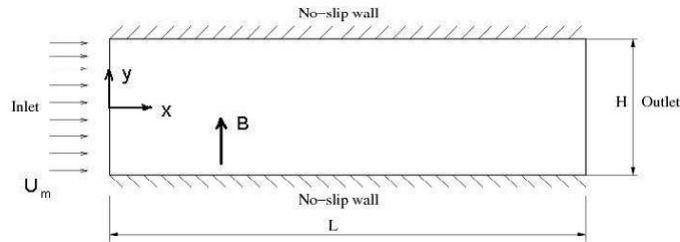


Figure 3.1: Hartmann flow

ization of plane Poiseuille flow in classical fluid mechanics. Let us consider a steady, laminar flow between two infinitely broad parallel plates as shown in Fig. (3.1). The fluid enters the channel with a uniform velocity whose magnitude is calculated as discussed below. The channel is infinitely long in the z -direction so that any variation of variables in this direction can be neglected and the flow is 2-D. A uniform magnetic

field is applied perpendicular to the channel walls. The flow becomes fully developed after some distance from the entry, so the velocity u and magnetic field \mathbf{B} depends only on the y coordinate. Chang and Lundgren[1] gave an analytical solution for both velocity and induced magnetic field as given below,

$$u(y) = \hat{u} \left[1 - \frac{\cosh(Hay)}{\cosh(Ha)} \right] \quad (3.1)$$

$$b(y) = \frac{-y}{Ha} + \hat{u} \frac{\sinh(Hay)}{\cosh(Ha)} \quad (3.2)$$

with characteristic magnitude of velocity

$$\hat{u} = \frac{1}{Ha} \frac{c + 1}{cHa + \tanh(Ha)} \quad (3.3)$$

where c is the wall conductance ratio, which depends on conductivity of the channel walls. The following input parameters are used for both analytical and numerical solutions.

- Length of the channel, $L = 80m$
- Height of the channel, $H = 2m$
- Grid points in the domain= 161×61

The inlet velocity which is given as uniform is calculated by averaging the profile (3.1) over the height of the channel. The analytical solutions (3.1) and (3.2) are non-dimensional while the numerical solution is dimensional. However, as the integrated non-dimensional velocity value is specified at the inlet, the numerical solution is automatically scaled to the non-dimensional value. Since the velocity has been scaled to the non-dimensional value the resulting magnetic field will also be scaled to non-dimensional value as both are coupled.

3.1.1 Hartmann flow with insulating walls

In case of insulating walls, the boundary conditions for electric potential ϕ is given as homogeneous Neumann on all walls (wall conductance ratio, $c = 0$ for insulating wall), for pressure, homogeneous Neumann at inlet and homogeneous Dirichlet at outlet are applied. For flow field no-slip conditions are applied at the wall and fully developed condition are applied at the outlet. Fig.(3.2) shows fully developed velocity

profile for different Hartmann number and result are considerably in good match with analytical solution.

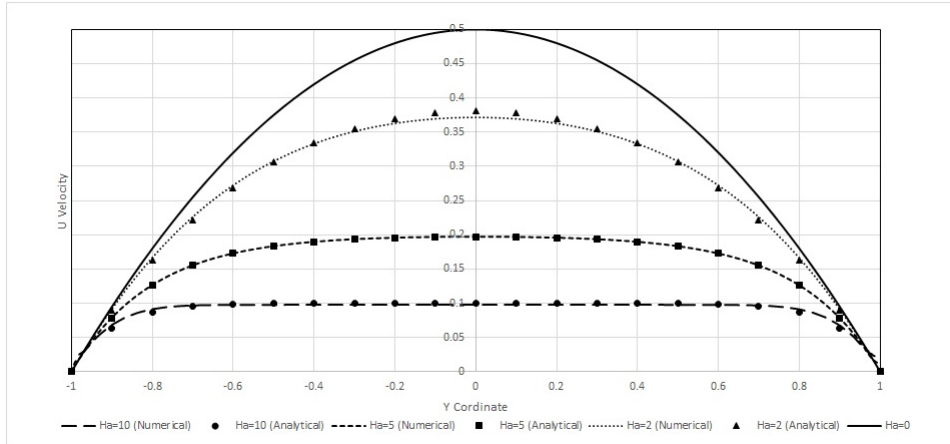


Figure 3.2: Velocity profiles for Hartmann flow for insulating walls

3.1.2 Hartmann flow with perfectly conducting walls

In case of perfectly conducting walls the boundary conditions for the electric potential ϕ on the walls is given as homogeneous Dirichlet (wall conductance ratio, $c = \infty$), while at the inlet and outlet of the channel homogeneous Neumann conditions are specified for ϕ . All other boundary condition are same as Hartman flow with insulating wall. Fig.(3.3) shows fully developed velocity profile for different Hartmann number and result are considerably in good match with analytical solution.

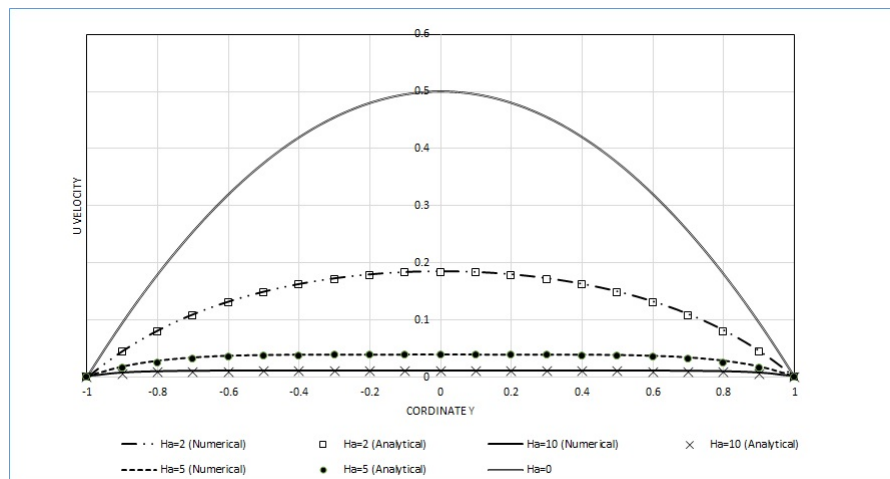


Figure 3.3: Velocity profiles for Hartmann flow for perfectly conducting walls

The following characteristic features can be identified from above graph.

- With increasing Hartmann number i.e. increase strength of magnetic field, the velocity profile flattens in the channel core and exhibits thin boundary layers near the Hartmann walls.
- The velocity decreases with increasing Hartmann number for both insulating and conducting wall.

3.2 Buoyancy driven convection in a rectangular cavity

Buoyancy driven magneto hydrodynamic flows are considered in the context of some magnetically confined fusion reactors using liquid metals as breeder and/or coolant. Here convective or forced flow is strongly opposed by the applied magnetic field. In these applications it may happen that the MHD damping is so large that convective heat transfer becomes a problem. During semiconductor crystal growth from melts one aims at establishing the fluid-solid interface conditions as homogeneous as possible. Time dependent flows as they might occur by buoyant convection should be avoided. One way to suppress instabilities or to minimize the velocities near the solidification front is the application of a magnetic field. To control the conditions of heat transfer during casting may be another application of magnetic fields to affect buoyant flows.

A suitable measure for buoyancy in hydrodynamic flows is the *Grashof number*,

$$Gr = \frac{g\beta\alpha L^4}{\nu^2}$$

which quantifies the importance of buoyant and viscous effects. The magnitude of the gravitational acceleration is denoted by g and L stands for a typical length scale of the problem. With the magnitude of a typical temperature gradient α the characteristic temperature difference of the problem becomes $\Delta T_0 = \alpha L$. All properties of the fluid like the kinematic viscosity ν or the electrical conductivity σ are assumed to be constant in the temperature range considered. The density of the fluid at the reference temperature T_0 is ρ_0 and the volumetric thermal expansion coefficient is β so that the density according to the *Boussinesq approximation* is described as

$\rho = \rho_0[1 - \beta(T - T_0)]$. The governing equation of the problem reads as,

$$\rho \left[\frac{\partial \mathbf{u}}{\partial t} + (\mathbf{u} \cdot \nabla) \mathbf{u} \right] = -\nabla p + \nu \rho \nabla^2 \mathbf{u} + \mathbf{J} \times \mathbf{B} + g\beta(T - T_0) \quad (3.4)$$

$$\left[\frac{\partial \mathbf{u}}{\partial t} + (\mathbf{u} \cdot \nabla) \mathbf{u} \right] = \alpha \nabla^2 T \quad (3.5)$$

The effect of a transverse magnetic field on buoyancy driven convection in a rectangular cavity was simulated for Grashoffs number 2×10^4 and Prandtl number 0.01 and domain of grid points 101. The flow domain is shown in Fig.(3.4). The cavity is thermally insulated on the top and bottom walls. Garandet et. al.[4] gave an analytical solution for the horizontal velocity along the vertical center line as,

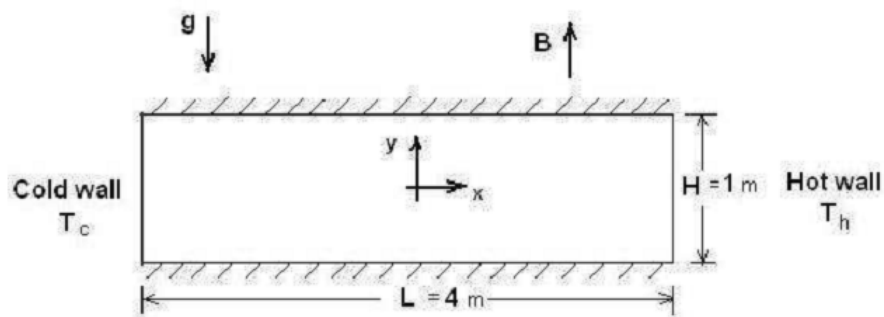


Figure 3.4: Schematic of buoyancy driven natural convection

$$u = \frac{Gr}{Ha^2} \left(\frac{\sinh Hay}{2 \sinh(Ha/2)} - 1 \right) \quad (3.6)$$

and in the absence of a magnetic field ($Ha = 0$) the profile is cubic given by Birikh[10];

$$u = \frac{Gr}{6} \left(y^3 - \frac{y}{4} \right)$$

Fig.(3.5) shows the temperature contour for different Hartmann number. For hartmann number 5 isotherm is more distorted and as increasing hartmann number the more distorted isotherm becomes straight gradually. This shows that convection does not play important role in the heat transfer and the heat transfer is more conductive in nature as Ha increases.

Fig.(3.6) shows comparison between numerical and analytical solution of horizontal velocity at the central vertical line of the cavity. Numerical solutions are in good agreement with analytical solution of Garandet. From Graph it is clear that velocity

increases from zero at the wall to a peak value and drop to zero at the center. As Hartmann number increases gradient of velocity become constant almost everywhere in the cavity except near the top and bottom wall called Hartmann layer.

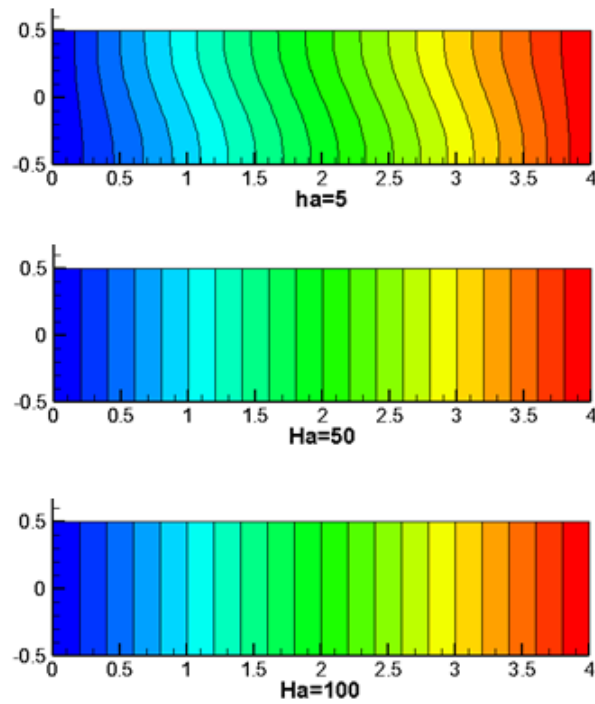


Figure 3.5: Temperature contour for different Hartmann numbers

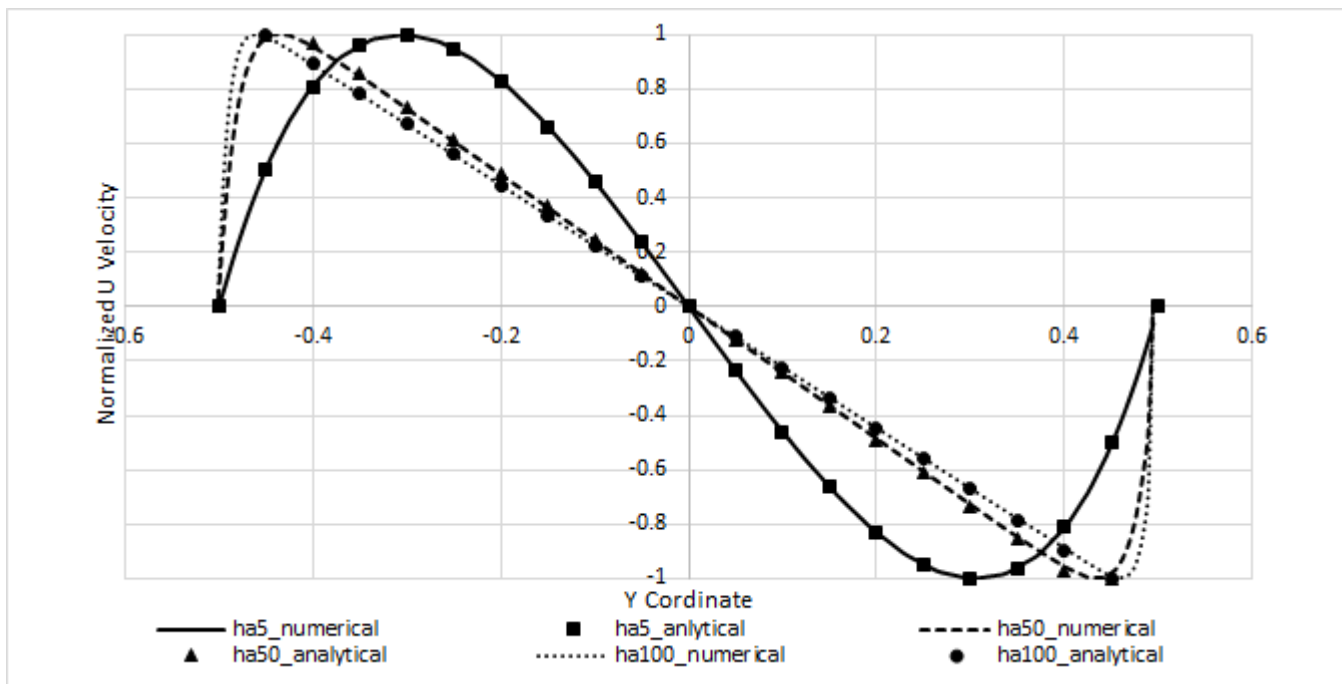


Figure 3.6: Normalized horizontal velocity along vertical centreline of the cavity for different Hartmann number

3.3 MHD flow in rectangular duct-Hunt's solution

To test the three dimensional validity of the code, MHD flow in 3D channel of rectangular cross section($25mm \times 25mm$) and $500mm$ length, with perfectly conducting walls perpendicular to the applied magnetic field and insulating walls parallel to the magnetic field considered by Hunt [2] was simulated for $Ha = 100$ and $Re = 679$.

The flow exhibits strong boundary layers at the walls. The layers formed at the wall parallel to the magnetic field are called side layers and have the thickness $\delta = 1/\sqrt{Ha}$. The layers that appear at the walls perpendicular to the magnetic field are called Hartmann layers and have a thickness $\delta = 1/Ha$. Numerical simulation was carried out in mesh of grid point $36 \times 26 \times 36$ and minimum of 4 grid points are ensured in boundary layers. A grid independence test had conducted in a higher resolution mesh ($46 \times 36 \times 46$) and the velocity is compared. The deviation of peak velocity is less than 0.5%.

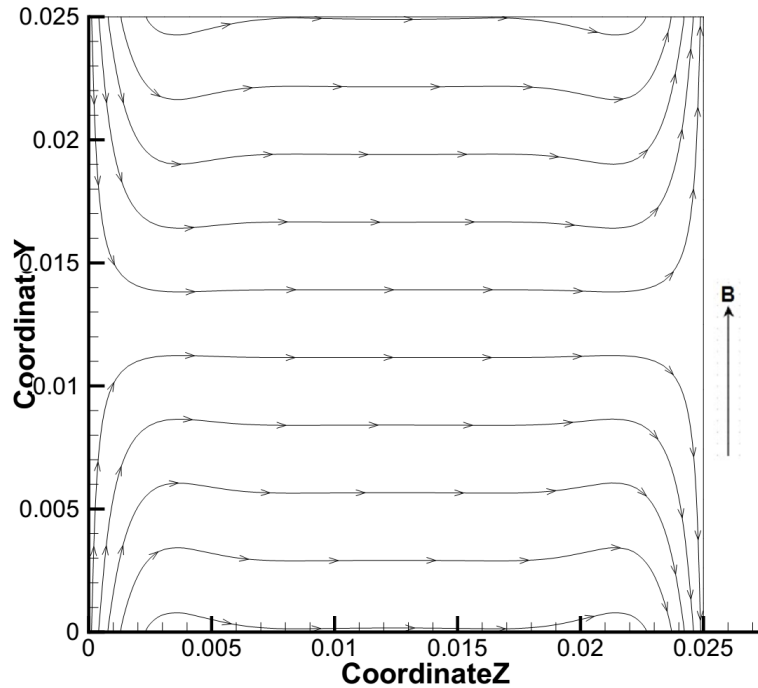


Figure 3.7: current density plot ($Ha=100$) at the outlet of the duct

From current density plot(Fig.3.7) it can be see that the current flows to the right-hand side in most of the duct's cross section. This region is called *core* of the flow. Because of the insulating side wall this current turns near the side wall through a narrow region called *side layer* and flows back to the left-hand side through hartmann wall since hartmann wall is perfectly conducting. Fig.(3.9) shows comparison of

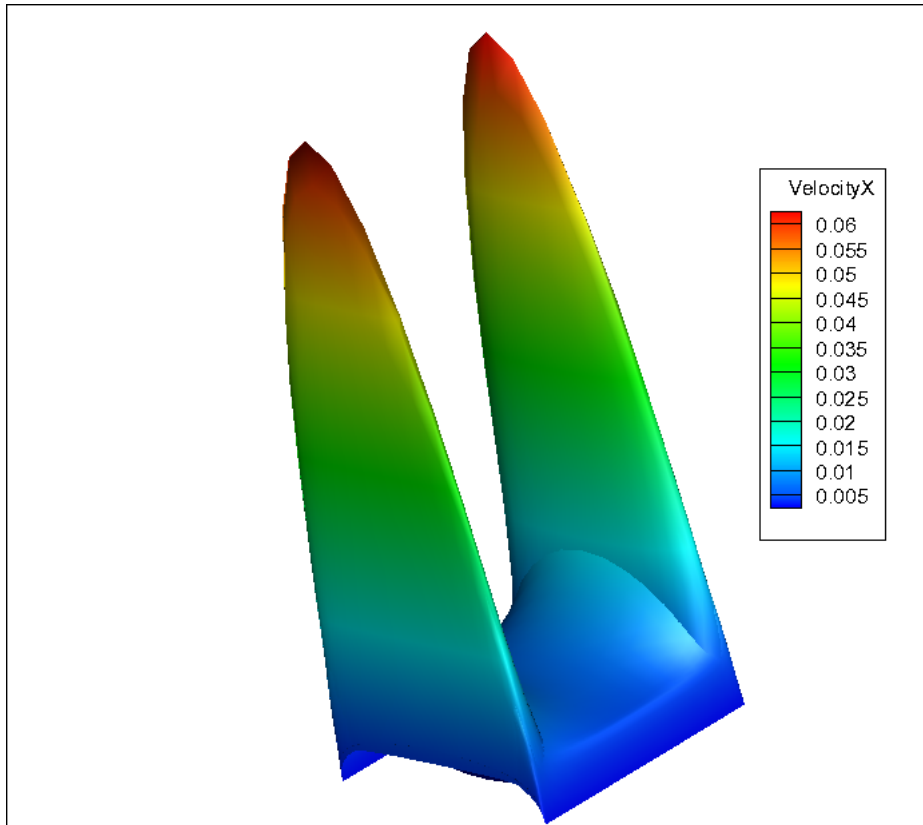


Figure 3.8: jet like velocity profile ($Ha=100$) at outlet of the duct.

velocity along side wall and deviation of peak velocity from Hunt analytical solution is less than 4.5%. This deviation may be due to limitation of numerical scheme or thin wall approximation of Hunt's solution. Jet like profile of velocity can be observed in Fig.(3.8).

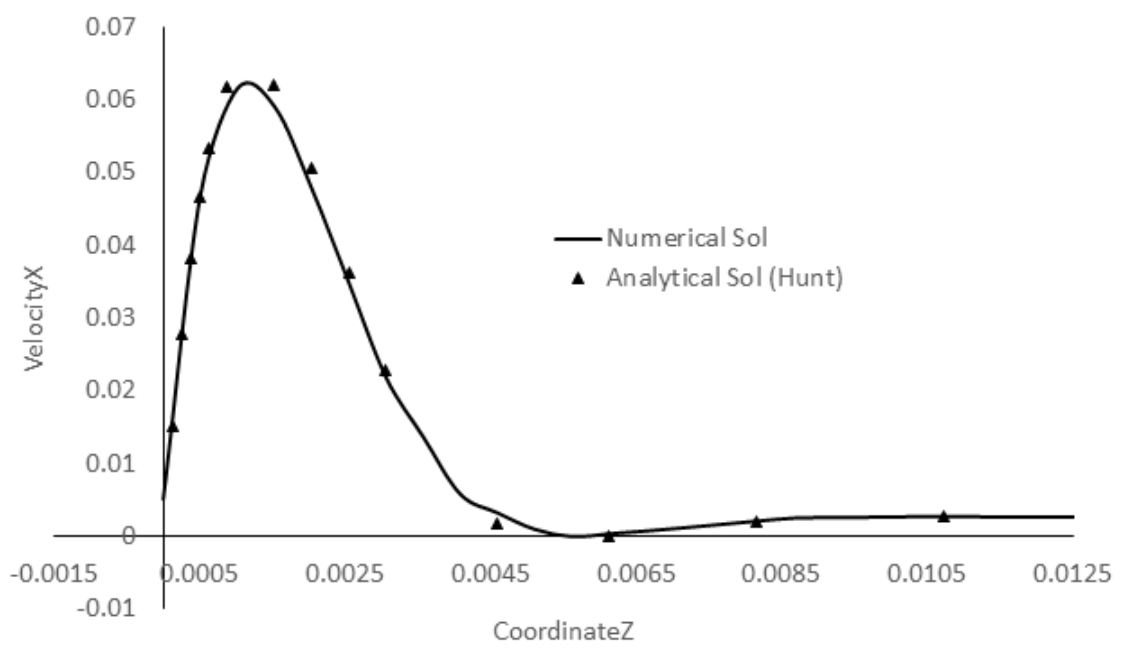


Figure 3.9: VelocityX comparison (Ha=100) along hartmann wall at the center of the duct.

Chapter 4

MHD flow through rectangular duct- effect of wall conductivity

This chapter discusses the effect of wall electrical conductivity on the velocity profile and pressure drop in a rectangular duct subjected to a transverse magnetic field. There are very few cases for which analytical solutions have been obtained for simple rectangular channel geometries.

1. Rectangular duct with insulating wall subjected to transverse magnetic field (Shercliff 1953)
2. Rectangular duct with perfectly conducting wall subjected to transverse magnetic field (Chang and Lundgren 1961; Uflyand 1961)
3. Rectangular duct with (1) Hartmann wall perfectly conducting and side wall with arbitrary conductivity and (2) side wall non-conducting and Hartmann wall with arbitrary conductivity (Hunt 1965).

So cases with walls of arbitrary conductivity have to be solved by numerical methods.

4.1 Laminar MHD flow in straight rectangular duct

Laminar MHD flow in rectangular straight duct are characterized by boundary layers and core flow as mentioned in section 2.8 and thickness of these boundary layer become smaller as Hartmann number increases. The resolution of these viscous layer makes the simulation of such flows at high Hartmann number a challenging task. A numerical simulation of straight rectangular duct with different arbitrary wall conductivity subjected to transverse magnetic field was carried out for Hartmann number 100

and 500 by solving complete Navier-stokes and Maxwell's equations using electrical potential formulation of Anupravaha solver.

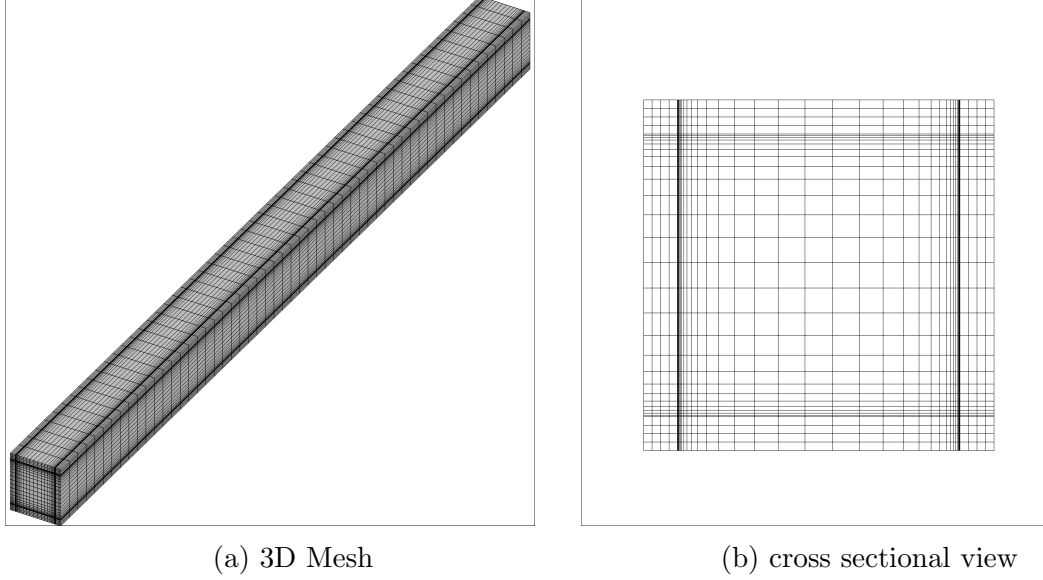


Figure 4.1: Computational domain

The simulation was carried out in a mesh of 36×36 grids in cross section and 41 grid in stream wise direction. The grid was refined towards the walls to obtain a good resolution of the boundary layers (Fig. 4.1) and a minimum of 4 grid points are ensured in these layer. Simulations were performed with a semi-coupled algorithm and uses the QUICK convective scheme. For the given Reynolds number the length of the domain is assumed to be enough to fully develop the flow. The following are the parameters used in the simulations.

- cross section of duct $= 25mm \times 25mm$
- Length of duct, $L = 500mm$
- Thickness of the wall, $t_{wall} = 3mm$
- Reynolds number of flow, $Re = 652$
- Hartmann number, $Ha = 100, 500$
- Uniform inlet velocity, $U_{avg} = 0.01m/s$
- Wall conductance ratio $c = \frac{\sigma_{wall} t_{wall}}{\sigma_{fluid} L}$

Figure. 4.2 shows current distribution for various wall conductance ratio ranging from insulating ($c = 0$) to perfectly conducting($c = \infty$). From the current density plots it can be seen that the current flows to the right-hand side in most of the duct's cross-section(*core*). Flow back to the left-hand side to close the circuit takes place only in narrow layers at the top and bottom walls called *Hartmann layer*, at the sidewalls, current flows mainly in the y-direction. Comparing pictures for different wall conductance ratios(Fig. 4.2a, 4.2b, 4.2c, 4.2d) we see that the current density rises when the conductance ratio increases.

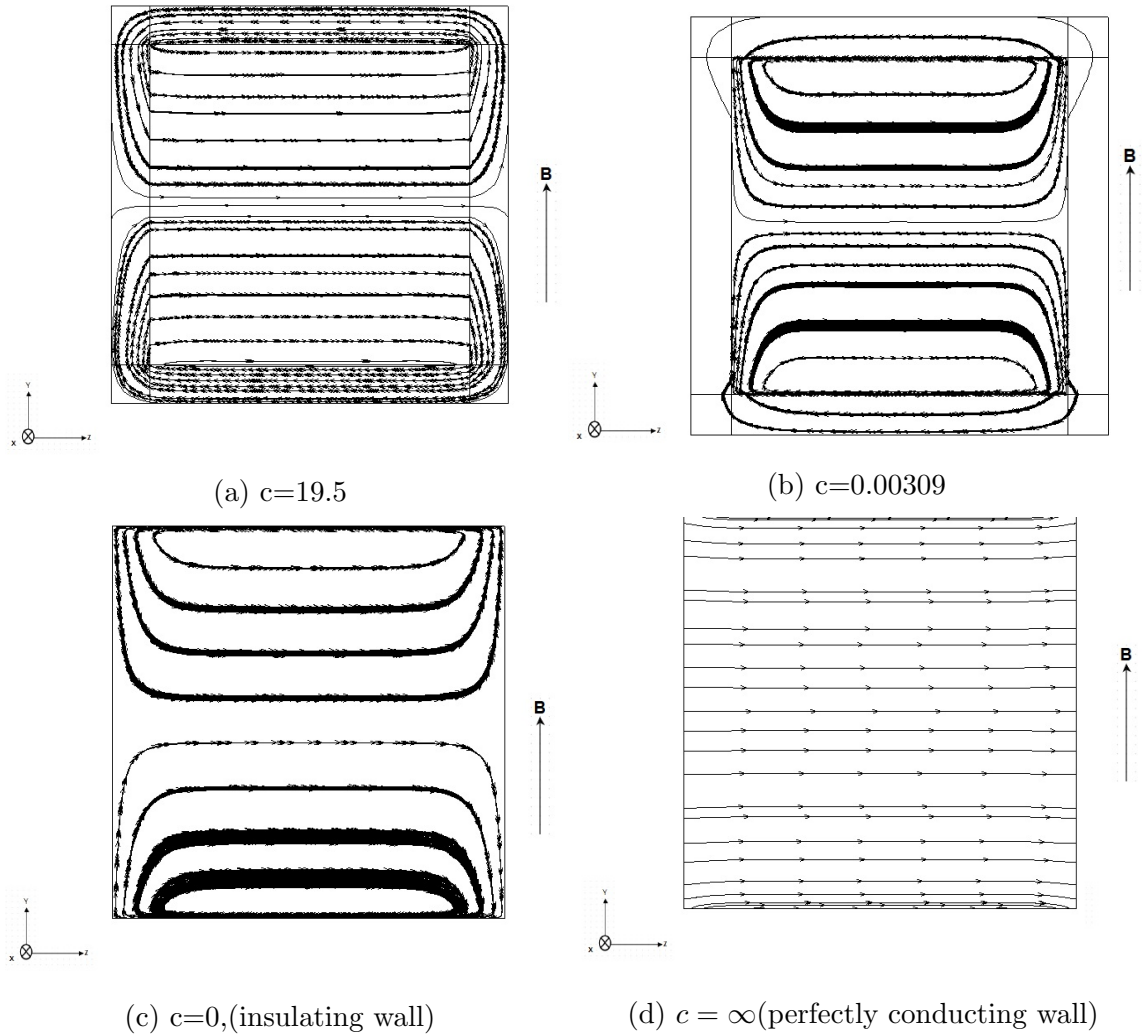


Figure 4.2: Current density stream traces at outlet for $Ha=100$

Looking at the velocities in Fig. 4.3 we easily find the three regions: Hartmann layer, and side layer and core. In the core, the velocity is nearly constant, abruptly falling to zero in the thin Hartmann layers which are at the walls perpendicular to the magnetic field. The most interesting region is the side layers which are at the walls

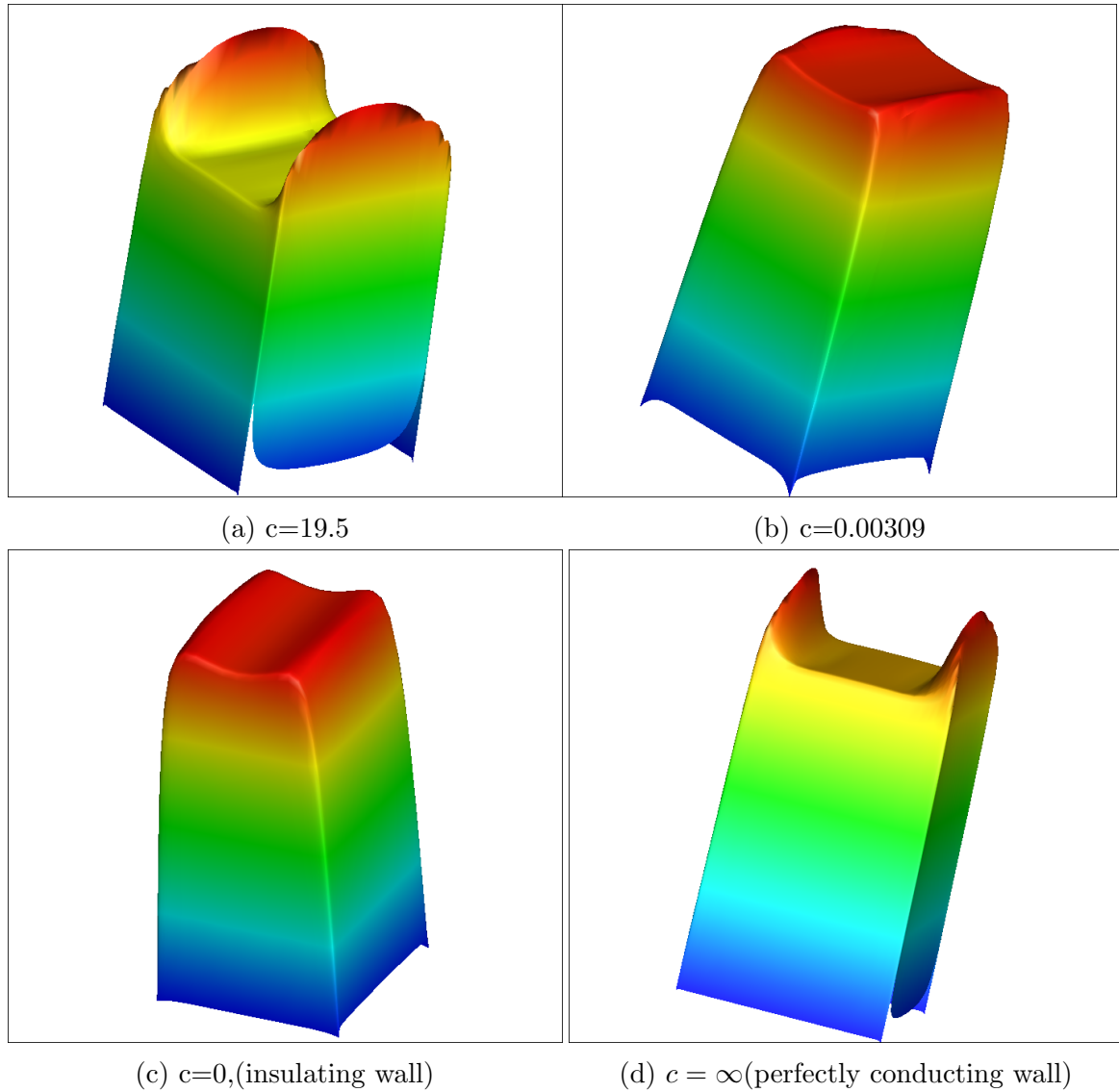


Figure 4.3: Velocity profile at outlet for $Ha=100$

perpendicular to the magnetic field. Their structure is strongly dependent on the wall conductance ratios and therefore on the current densities. The larger the current densities, the higher the velocities are in the side layers, forming the so-called M-shaped profiles. The explanation of this striking phenomenon is straightforward (Hunt 1965). In the side layers the current density always has a component j_y parallel to B_0 , the applied magnetic field. It does not contribute to the Lorentz force $j \times B_0$, acting against the flow. On the other hand, in the core j_y vanishes, and the whole current contributes to $j \times B_0$, leading to a higher force on the core flow. This component j_y depends on the conductivity of side wall. For the insulating case, current has to pass through the thin side layer which offer higher resistance, leads to less $j \times B_0$ and

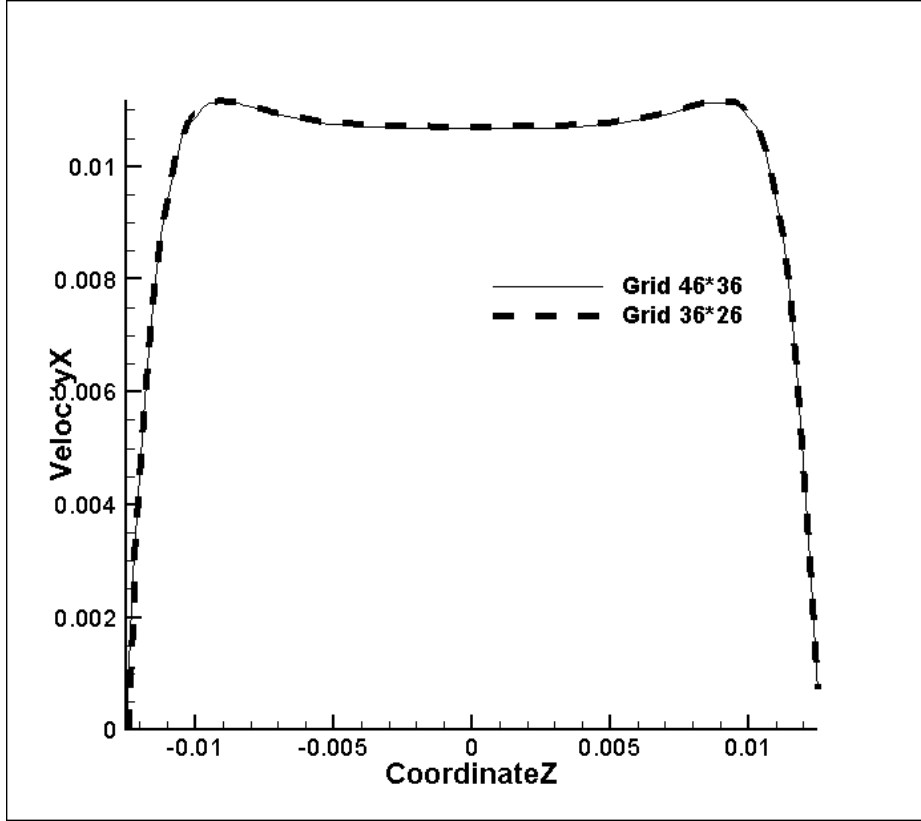


Figure 4.4: Velocity profile of the MHD flow in a square duct at $Ha = 100$, $c = 0.00309$ along the centerline perpendicular to the magnetic field (Grid independence test)

higher velocity and consequently a flat velocity profile(Fig. 4.3b, 4.3c). In the case of a conducting wall current can pass through conducting side wall which offer least resistance leads larger Lorentz force at the core and lesser core velocity. However, in the side layer the retarding force is nearly zero (as j and B are parallel) and velocity is high, leads to a jet like profile(Fig. 4.3a, 4.3d).

For grid independence test, the velocity profile from grids of 46×36 and 36×26 in cross section for a wall conductance ratio $c=0.00309$, are compared and deviation of peak velocity is less than 0.6% and insignificant deviation in core. Fig. 4.4 shows the comparison.

Table. 4.1 shows the values of pressure gradient for different values of Hartmann number and wall conductivity ratio. The results shows that the pressure gradient increases steeply with Hartmann number and decrease with wall conductance ratio, with the insulated wall case having the lowest pressure drop.

In Anupravaha the Lorentz force is evaluated at the n^{th} level while all the other terms are discretized at the $n + 1$ level. This leads to a constraint on the time step at high Interaction parameters as $\Delta t \approx 1/N$ especially high values N . As Hartmann

Table 4.1: Pressure gradient for Ha=100, Re=652 for different wall conductance ratio

Sl.No	Wall conductance ratio(c)	Pressure gradient (N/m)	
		Ha=100	Ha=500
1	∞	1126.43	
2	19.5	991.765	21009
3	2.16	690.266	16754.7
4	0.24	192.371	3949.89
5	0.003	15.8669	150.593
6	0	12.6393	70.5861

number increases, in order to resolve boundary layers properly, the total number of grids in the domain will increase. So numerical simulation of MHD flow at high Hartmann numbers also take longer computation time.

Chapter 5

MHD flow in rectangular duct-fully developed solution

This chapter describe the numerical study of the laminar, incompressible flow of a conducting fluid in a rectangular duct under a uniform magnetic field at very high Hartmann number in fully developed flow regime.

5.1 Formulation of the problem

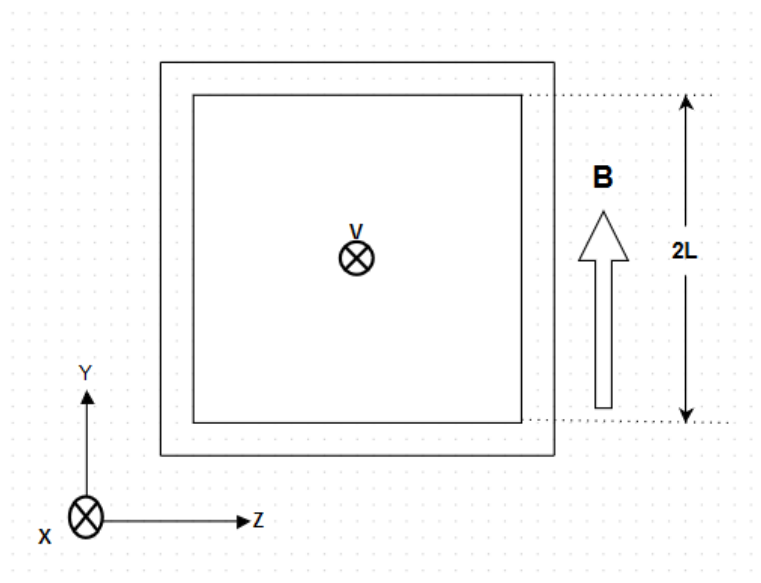


Figure 5.1: Cross-Sectional view of the square duct used for the study

Let us consider a unidirectional, incompressible flow, of an electrically conducting fluid through a rectangular duct of characteristic length L , (half distance between

the Hartmann walls). An external magnetic field $\mathbf{B} = B_0\hat{y}$ is imposed, and the flow is driven by a uniform pressure gradient in the axial direction, $\nabla p = -f\hat{x}$. For channels with constant cross section a fully developed flow establishes where the velocity $v = u(y, z)\hat{x}$ has only one non-zero component depending on the lateral coordinates y and z .

To obtain non-dimensional equation, we scaled the governing equations

$$\rho \left[\frac{\partial \mathbf{u}}{\partial t} + (\mathbf{u} \cdot \nabla) \mathbf{u} \right] = -\nabla p + \nu \rho \nabla^2 \mathbf{u} + \mathbf{J} \times \mathbf{B}$$

$$\mathbf{J} = \sigma(-\nabla\phi + \mathbf{u} \times \mathbf{B})$$

$$\nabla^2\phi = \nabla \cdot (\mathbf{u} \times \mathbf{B})$$

by using non dimensional variable as, $\nabla^* = (1/L)\nabla, z^* = z/L, y^* = y/L, u^* = u/U, B^* = B/B_0, t^* = t\sigma B_0^2/\rho, J^* = J/\sigma U B_0, p^* = p/\sigma U L B_0^2, \phi^* = \phi/U B_0 L$. For fully developed flow the convective transport term of the momentum equation become zero and the governing equations in non-dimensional form (omitting stars in all term after substitution) can be read as,

$$\frac{\partial \mathbf{u}}{\partial t} = -\nabla p + \frac{1}{Ha^2} \nabla^2 \mathbf{u} + \mathbf{J} \times \mathbf{B} \quad (5.1)$$

$$\mathbf{J} = -\nabla\phi + \mathbf{u} \times \mathbf{B} \quad (5.2)$$

$$\nabla^2\phi = -\frac{\partial u}{\partial z} \quad (5.3)$$

Substituting equation 5.2 in 5.1 we will get momentum equation in x-direction as

$$\frac{\partial \mathbf{u}}{\partial t} = -\nabla p + \frac{1}{Ha^2} \nabla^2 \mathbf{u} + \mathbf{B} \left(\frac{\partial \phi}{\partial x} \mathbf{B} - u \mathbf{B} \right)$$

We can solve the equations assuming a unit pressure gradient and get a corresponding velocity profile. So we are essentially solving the above equation as

$$\frac{\partial \mathbf{u}}{\partial t} = -1 + \frac{1}{Ha^2} \nabla^2 \mathbf{u} + \mathbf{B} \left(\frac{\partial \phi}{\partial x} \mathbf{B} - u \mathbf{B} \right)$$

and if we multiply above by α , some constant, since the equation is linear, all variables will get multiplied by α and so the pressure drop required for a specific flow rate

$(Q_{specific})$ become α and

$$Q_{specific} = \int_{-1}^1 \int_{-1}^1 u dy dz = \alpha Q_p$$

$$\alpha = \frac{Q_{specific}}{Q_p} \quad (5.4)$$

where Q_p is the flow rate due to unit pressure gradient. In our case the area of cross section is 2×2 so α can be written as

$$\alpha = \frac{Q_{specific}}{Q_p} = \frac{4U_{specific}}{4U_p} = \frac{U_{specific}}{U_p}$$

where U_p is the average velocity due to unit pressure gradient and which can be calculated from velocity profile. In the coming discussions, given values of the pressure gradient are pressure gradient due to unit average velocity ($U_{specific} = 1.0, Q_{specific} = 4$).

The flow is essentially a two-dimensional and parameter affecting the flow is Hartmann number and wall conductivity ratio, $c = \frac{\sigma_w t_w}{\sigma L}$, where σ is the electrical conductivity of the fluid, σ_w is the electrical conductivity of the wall and t_w is the thickness of the wall.

5.2 Boundary conditions and input parameters

Inlet and outlet

Inlet and outlet is in fully developed region, so homogeneous Neumann boundary condition is applied for all velocity components and electrical potential ϕ . Since flow is driven by unit pressure gradient, unit pressure is applied at the inlet zero pressure is applied at the outlet.

Walls

For velocity homogeneous Dirichlet boundary conditions and for pressure homogeneous Neumann is applied. For electrical potential ϕ homogeneous Neumann boundary condition is applied at the outer surface, while current continuity $\sigma_{fluid} \left(\frac{\partial \phi}{\partial n} \right)_{fluid} = \sigma_{solid} \left(\frac{\partial \phi}{\partial n} \right)_{solid}$ is applies at fluid solid interface.

Input parameters

The following parameters are given in accordance with non-dimensional governing equation

- Density of fluid=1.0
- Dynamic Viscosity of fluid= $\frac{1}{Ha^2}$
- Electrical conductivity of fluid=1.0
- Electrical conductivity of walls= $10 \times c$, c is the wall conductance ratio ($c = \frac{\sigma_{wall}t_{wall}}{\sigma_{fluid}L} = \frac{\sigma_{wall} \times 0.1}{1.0 \times 1}$).
- Strength of imposed magnetic field $B=1.0$

5.3 Grid and Computational detail

Numerical simulations were carried out in a square geometry of cross sectional area 2×2 and one cell (of unit length) in stream-wise direction. Both Hartmann layer and side layer are resolved properly to capture the current flowing through it. Number of grid points in the cross section was 101×101 (Fig. 5.2) and one grid point in stream-wise direction. In this method the number of grid points is very less compared to solving the full domain (including entrance region) and here the momentum equation is linear leading to quicker convergence of the solution. Because the inertia-less approach is used, we need not to solve for mass fluxes, which again resulting in lower computation time.

5.4 Comparison with full solution

Numerical simulation of inertia-less method was compared with full solution for Hartmann numbers 100, 500, 1000, 1298 and wall conductance ratio $c = 0.01546$, for a non-dimensional flow rate of 4. (Full solution result are taken from Narendra Gajbhiye, Unpublished). Fig. 5.3- 5.6 shows the comparison of normalized u-velocity profile (normalized by average duct velocity) along center line perpendicular to applied magnetic field for different Hartmann number and the results match very well. Table. 5.1 shows the comparison of numerical values of the pressure gradient (non-dimensional) for the non dimensional flow rate of 4. This inertia-less simulation took less than two days to reach the steady state solution the while full solution takes around two weeks

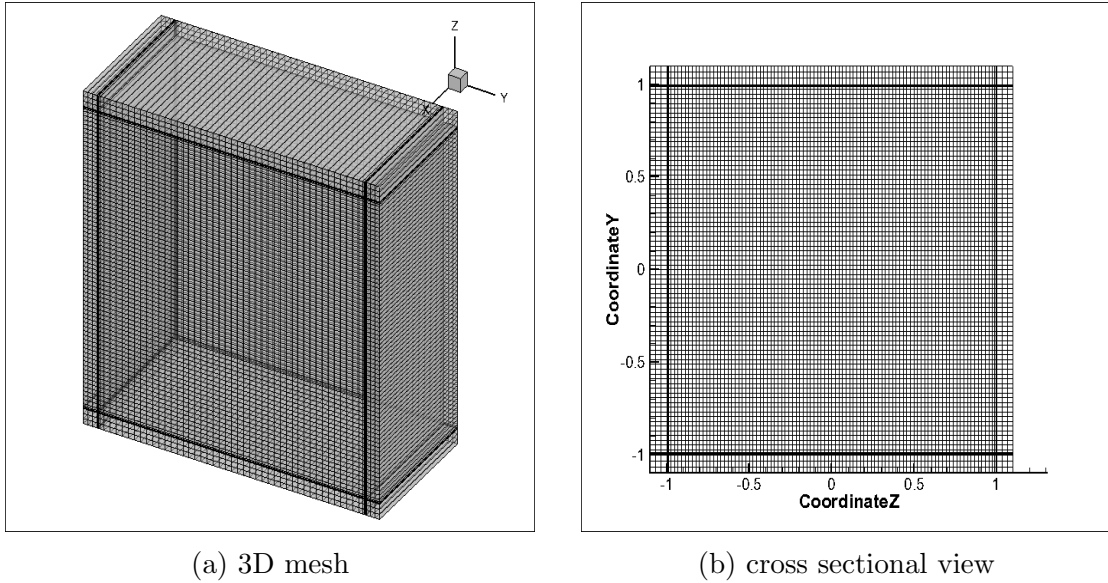


Figure 5.2: Grid used for numerical simulation, $Ha=10000$

on the same processor. So if we are not interested in what happening in the entrance region, to get the flow profile and pressure drop due to the MHD effect, this method give accurate results using much less computational resources.

Table 5.1: Non dimensional pressure gradient for $Ha=100, 500, 1000, 1298$

Hartmann number	Inertia-less solution	Full solution
100	0.12376	0.1243
500	0.10986	0.109005
1000	0.108265	0.106369
1298	0.107355	0.103418

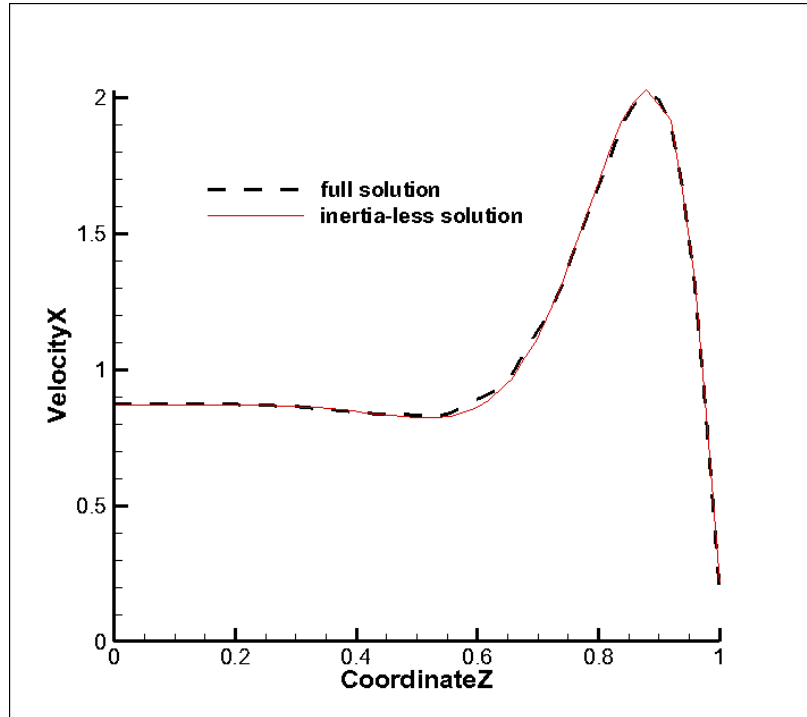


Figure 5.3: Normalized velocity profile along center line perpendicular to magnetic field for $Ha=100$, $c=0.01546$

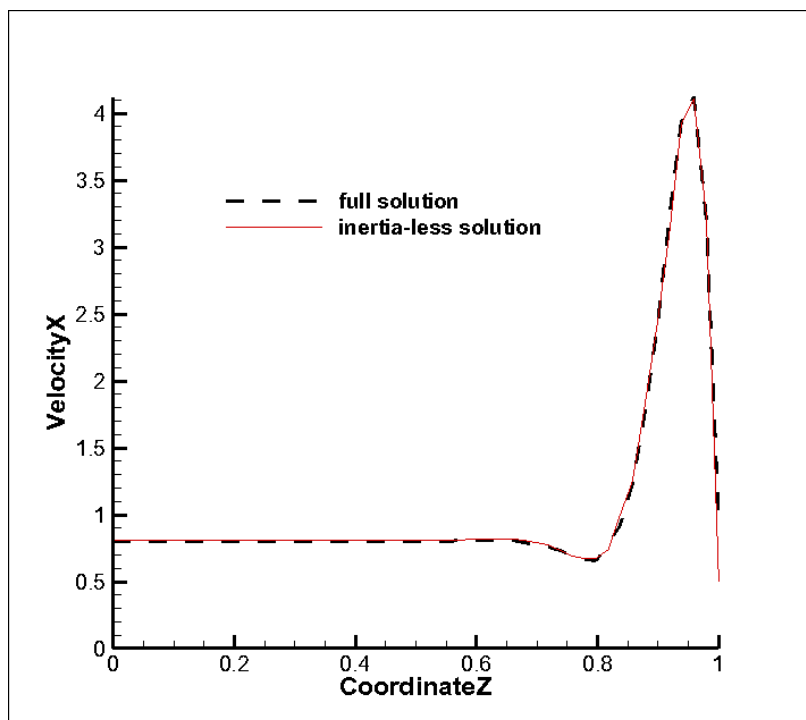


Figure 5.4: Normalized velocity profile along center line perpendicular to magnetic field for $Ha=500$, $c=0.01546$

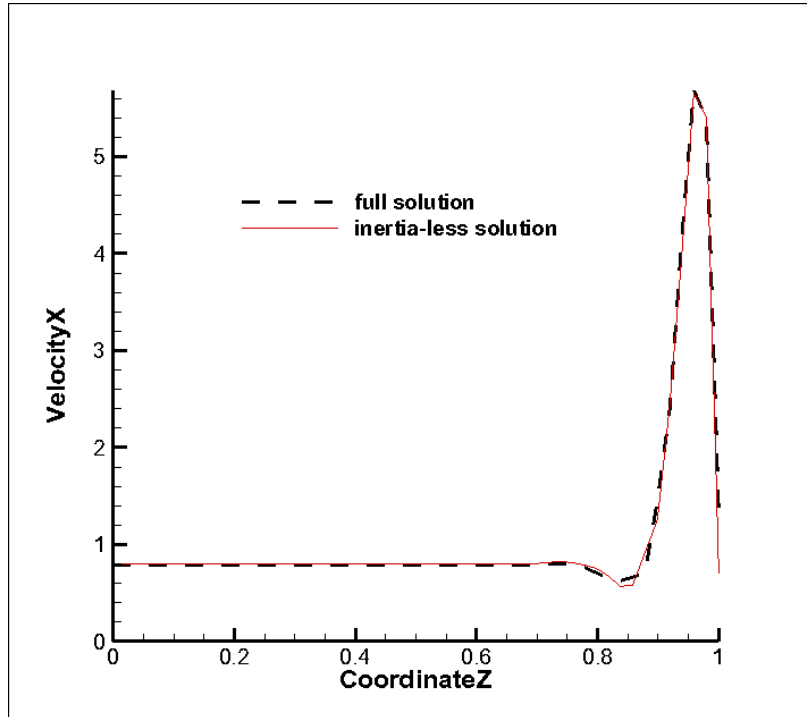


Figure 5.5: Normalized velocity profile along center line perpendicular to magnetic field for $Ha=1000$, $c=0.01546$

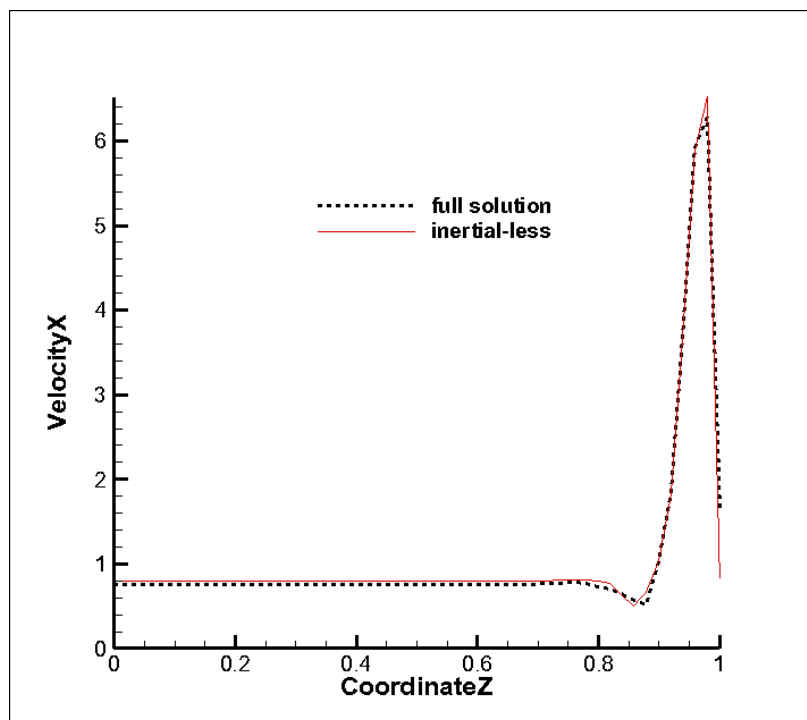


Figure 5.6: Normalized velocity profile along center line perpendicular to magnetic field for $Ha=1298$, $c=0.01546$

5.5 Fully developed flow solution at very high Hartmann number

Validation with Hunt's case

To validate the inertia-less approach, a numerical simulation for the flow through a rectangular duct (2×2) and of wall thickness=0.1 was carried out. The conductance ratio $c = 0.05$ for the Hartmann walls, while the side walls are insulated. An analytical solution exists for this case (case 2 of Hunt, [2]) with which results are compared and the deviation of peak velocity from analytical result is 3.2%. A distinguishable jet-like velocity profile can be seen in Fig.(5.8). The velocity in the side layer is compared with the analytical solution in Fig. 5.7. The results are seem to be quite good for the very $Ha=10000$ of the computation.

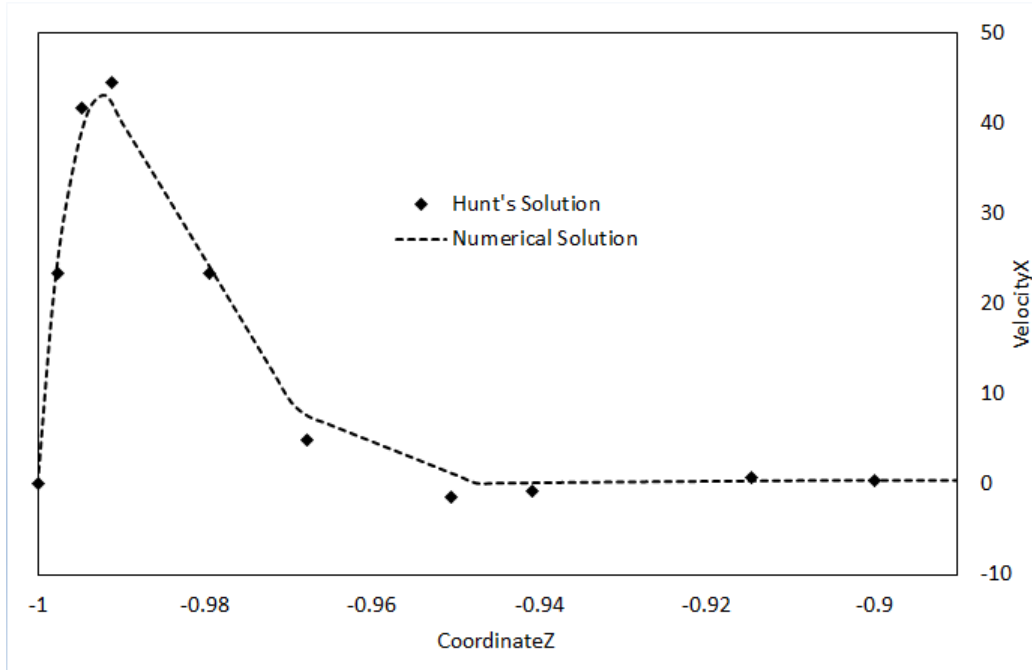


Figure 5.7: Comparison of normalized velocity profile along center line perpendicular to magnetic field for $Ha=10000$

	Peak velocity	Core velocity
Hunt's solution	44.51724	0.344828
Numerical solution	43.08023	0.443532

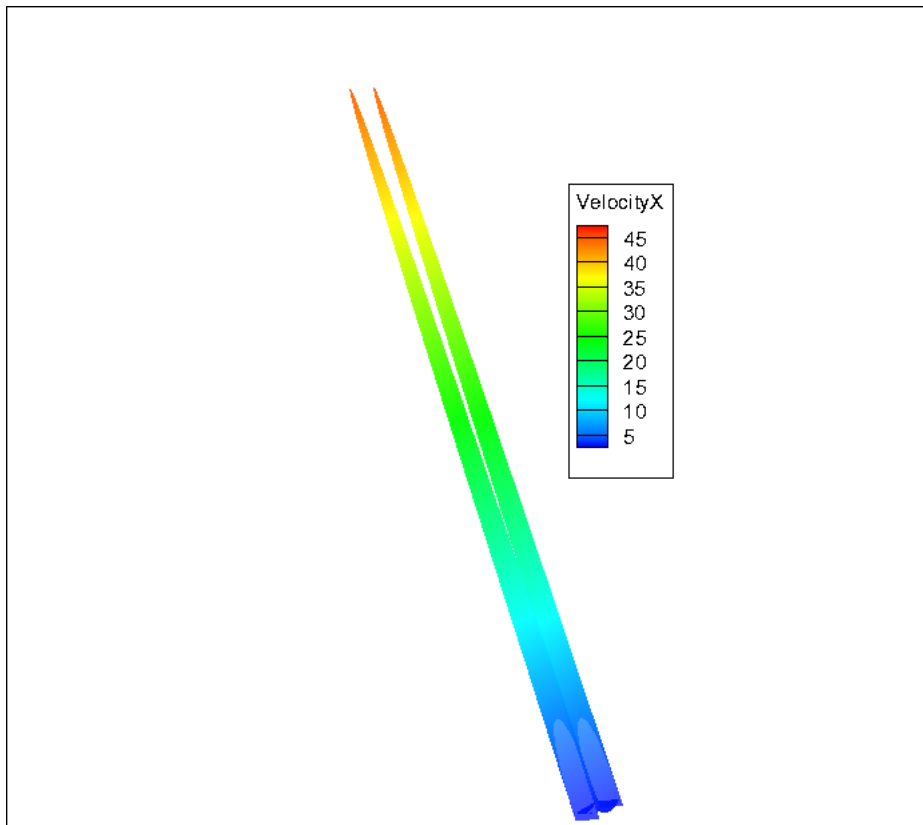


Figure 5.8: jet-like profile for Hunt's case for $Ha=10000$

Rectangular duct with arbitrary wall conductivity

Numerical simulations of MHD flow in rectangular duct with arbitrary wall conductivity were carried out at very high Hartmann numbers which is very relevant to fusion engineering applications, in a geometry of cross-sectional area 2×2 and unit length in stream-wise direction. Number of grid points in the cross section was 121×121 and one grid point in stream-wise direction and minimum of 5 grid points were ensured in the boundary layer ($\sim 1/Ha$). The variables have been rescaled in the same way as above and result of simulation are shown for Hartmann number $10^4, 1.5 \times 10^4, 2 \times 10^4, 3 \times 10^4$ and wall conductance ratio $c = 0, 2, 20$.

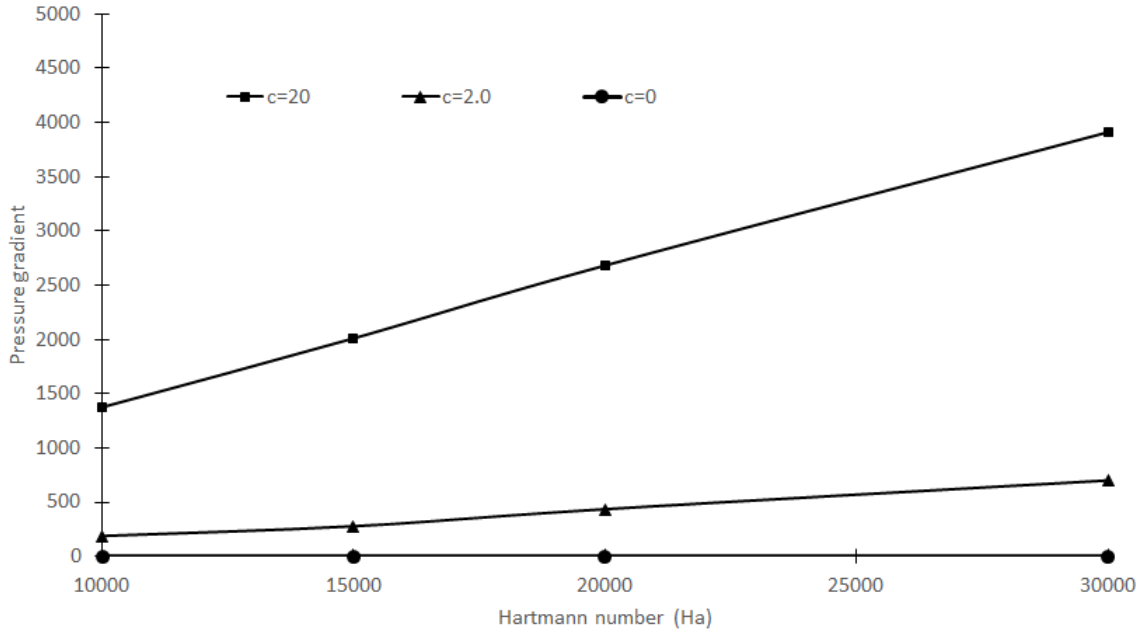


Figure 5.9: Pressure gradient in a square duct as a function of the Hartmann numbers (Ha)

Fig. 5.12 shows pressure drop in a rectangular duct as function of Hartmann number for a non-dimensional flow rate of 4. It is clearly seen that perfectly conducting walls result in significantly higher MHD pressure losses and from equation. 5.4 it can be conclude that given Hartmann number the volumetric flow rate is largest in a channel with electrically insulating walls and smallest for perfectly conducting walls. Fig. 5.14 shows velocity profile in the side layer and well known jet-like profile can be seen whereas in the insulating case flat profile can be seen in Fig. 5.13 for different hartmann numbers.

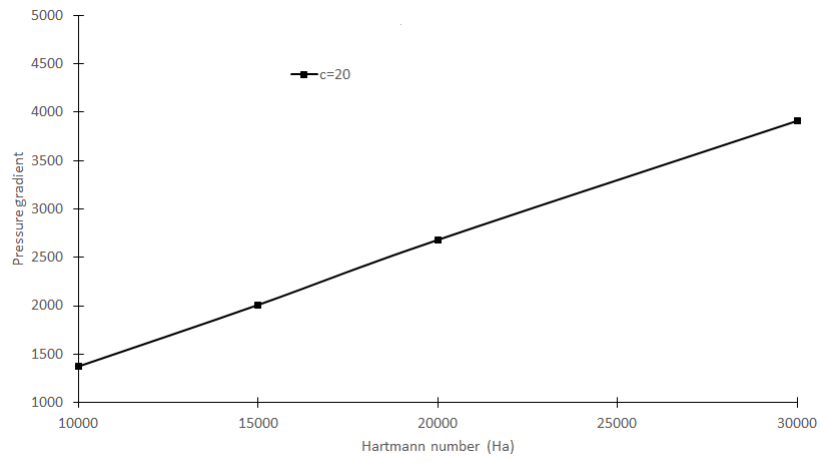


Figure 5.10: Pressure gradient in a square duct as a function of the Hartmann numbers (Ha) for $c=20$

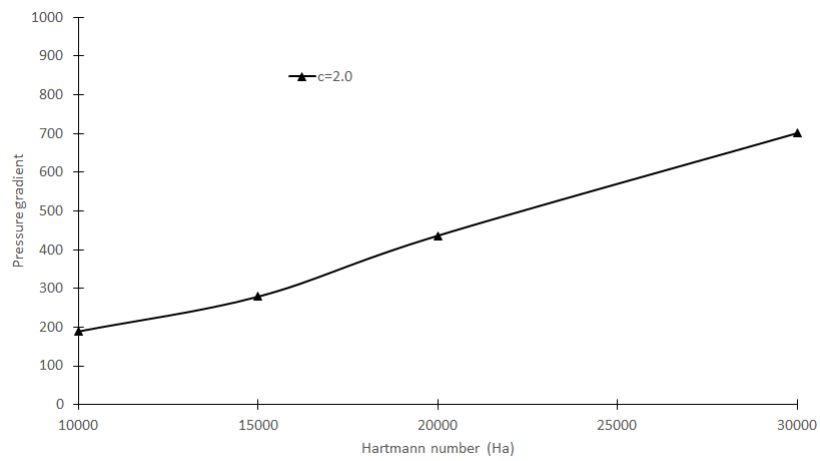


Figure 5.11: Pressure gradient in a square duct as a function of the Hartmann numbers (Ha) for $c=2.0$

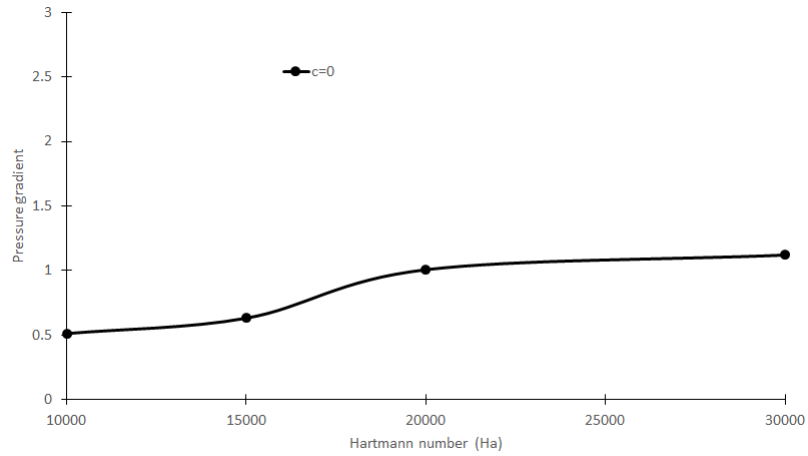


Figure 5.12: Pressure gradient in a square duct as a function of the Hartmann numbers (Ha) for $c=0$

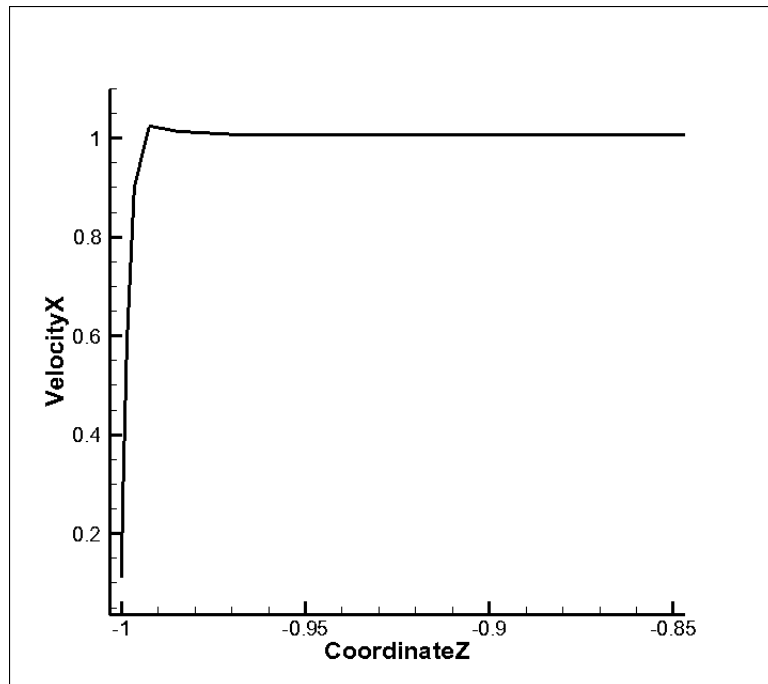
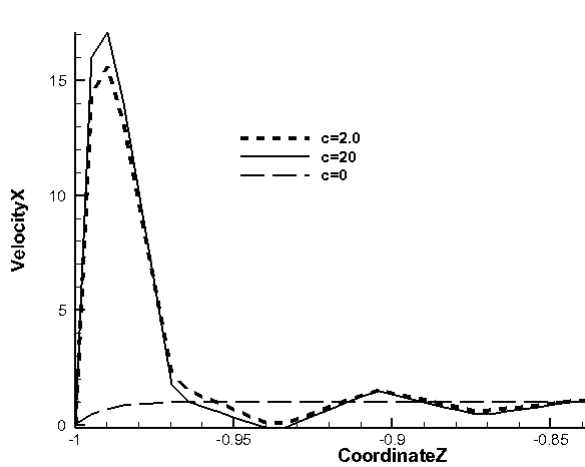
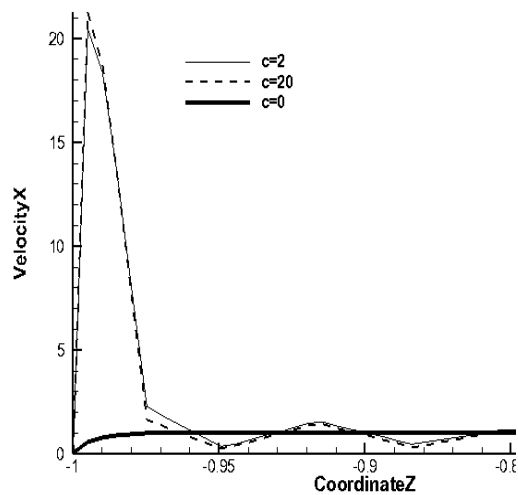


Figure 5.13: Normalized velocity profile along center line perpendicular to magnetic field for wall conductance ratio(c)=0, Ha

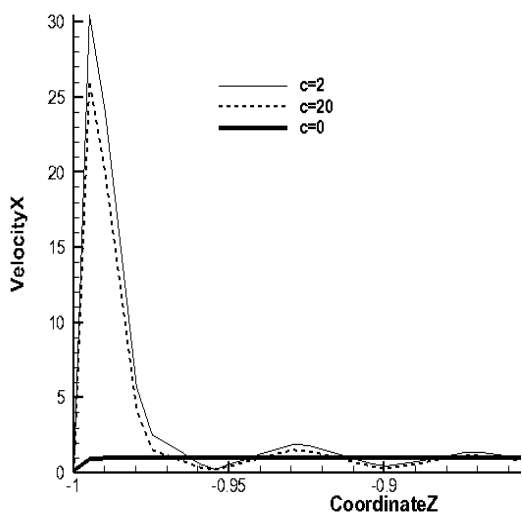
Since flow is fully developed the pressure drop required for any flow rate can be found by multiplying the corresponding average velocity with pressure gradient due to unit average velocity.



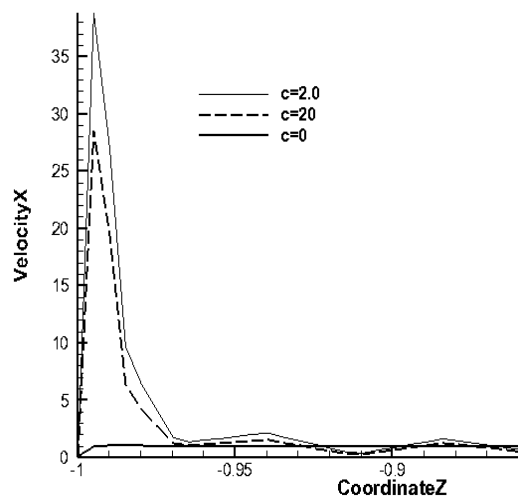
(a) $Ha=10000$



(b) $Ha=15000$



(c) $Ha=20000$



(d) $Ha=30000$

Figure 5.14: Normalized velocity profile along center line perpendicular to magnetic field for different Hartmann numbers

Chapter 6

Conclusion

In the present work, electrical potential formulation (induction-less) of Anupravaha MHD module is used for study of MHD flow in rectangular duct with arbitrary wall conductivity, and it is found that MHD pressure drop largely depends on wall conductivity. Numerical simulation of these flow using complete Navier-Stokes and allied equations require huge computational resources especially at High Hartmann number due to the following reasons.

- Error in current density(J) is amplified by N , the interaction parameter, in momentum equation when used to calculate momentum equation. So time step should be $\approx 1/N$. So as N increases time required to reach steady state will increase.
- Suitable resolution of MHD boundary layers and smooth transition between various region (core-region) is required. So by increasing Hartmann number, total number of nodes becomes larger.

If we are not interested in what happening in the entrance regime, it is not necessary to solve complete 3D Navier-Stoke's equation to get flow profile and pressure gradient in a constant area duct. So inertia-less method is used to simulate fully developed region of rectangular duct with arbitrary wall conductivity at very high Hartmann number.

The results of inertial-less method compared with solutions from complete 3D Navier-Stoke's equation (for $Ha=1298$, which took four weeks to reach steady state) and results are matching perfectly. The assumption of fully developed flow enormously reduces the amount of computation as the flow does not change in the longitudinal direction. This allows us to have only one cell in that direction whereas in

developing flows we may need several hundred cells . This allows us to do the computation for for very high Hartmann number flows ($\sim 10^4$), which would otherwise be impossible.

Using inertia-less method, parametric study of laminar MHD flow in a square duct at very high Hartmann number (upto 30000) have conducted and graph of non dimensional pressure gradient, as a function of Hartmann number for various wall conductance ratio is given which can be used to calculate MHD pressure drop required to obtain a specific flow rate.

References

- [1] C. Chang and Lundgren. Duct flow in magnetohydrodynamics. *Zeitschrift fur angewandte Mathematik und Physik* XII, (1961) 100– 114.
- [2] J. Hunt. Magnetohydrodynamic flow in rectangular ducts. *Journal of Fluid Mechanics* 21, (1965) 577–590.
- [3] J. Walker. Magnetohydrodynamic duct flows in rectangular ducts with thin conducting walls. *I.J.Mec* 20, (1981) 79– 112.
- [4] J. Garandet, T. Alboussiere, and R. Moreau. Buoyancy driven convection in a rectangular enclosure with a transverse magnetic field. *International Journal of Heat and Mass Transfer* 35, (1992) 741 – 748.
- [5] H. BEN HADID and D. HENRY. Numerical study of convection in the horizontal Bridgman configuration under the action of a constant magnetic field. Part 2. Three-dimensional flow. *Journal of Fluid Mechanics* 333, (1997) 57–83.
- [6] H. Ozoe and K. Okada. The effect of the direction of the external magnetic field on the three-dimensional natural convection in a cubical enclosure. *International Journal of Heat and Mass Transfer* 32, (1989) 1939 – 1954.
- [7] I. D. Piazza and M. Ciofalo. {MHD} free convection in a liquid-metal filled cubic enclosure. I. Differential heating. *International Journal of Heat and Mass Transfer* 45, (2002) 1477 – 1492.
- [8] C. Karcher, Y. Kolesnikov, O. Andreev, and A. Thess. Natural convection in a liquid metal heated from above and influenced by a magnetic field. *European Journal of Mechanics-B/Fluids* 21, (2002) 75–90.
- [9] U.Muller and L.Buhler. Magnetofluidynamics in Channels and Containers. 2nd edition. Springer-Verlag, 2001.

- [10] R. Birikh. Thermocapillary convection in a horizontal layer of liquid. *Journal of Applied Mechanics and Technical Physics* 7, (1966) 43–44.
- [11] N. Vetcha. Numerical Simulation of Liquid Metal MHD Flows. Master’s thesis, IIT Kanpur 2007.
- [12] R. Paniharam. Numerical Simulation of Liquid Metal MHD Flows with Imposed and Induced Magnetic Field. Master’s thesis, IIT Kanpur 2008.
- [13] J. A. Shercliff. The flow of conducting fluids in circular pipes under transverse magnetic fields. *Journal of Fluid Mechanics* 1, (1956) 644–666.
- [14] J. A. Shercliff. Magnetohydrodynamic pipe flow Part2. High Hartmann number. *Journal of Fluid Mechanics* 13, (1962) 513–518.